Miner Deposita (2006) 41: 301–321
DOI 10.1007/s00126-006-0062-x

ARTICLE

Agnès Markowski · Jean Vallance · Massimo Chiaradia · Lluìs Fontboté

Mineral zoning and gold occurrence in the Fortuna skarn mine, Nambija district, Ecuador

Received: 24 February 2005 / Accepted: 25 March 2006 / Published online: 31 May 2006

Abstract The Fortuna oxidized gold skarn deposit is located in the northern part of the Nambija gold district, southern Ecuador. It has been subdivided into four mineralized sites, covering a distance of 1 km, which are named from north to south: Cuerpo 3, Mine 1, Mine 2, and Southern Sector. Massive skarn bodies occur in K–Na metasomatized volcanic and volcaniclastic rocks of the Triassic Piuntza unit. They appear to result from selective replacement of volcaniclastic rocks. Very minor presence of bioclast relicts suggests the presence of subordinate limestone. Endoskarn type alteration with development of Na-rich plagioclase, K-feldspar, epidote, actinolite, anhedral pyroxene, and titanite affects a quartz–diorite porphyritic intrusion which crops out below the skarn bodies in Mine 2 and the Southern Sector. Endoskarn alteration in the intrusion grades into a K-feldspar ± biotite ± magnetite assemblage (K-alteration), suggesting that skarn formation is directly related to the quartz–diorite porphyritic intrusion, the latter being probably emplaced between 141 and 146 Ma. The massive skarn bodies were subdivided into a dominant brown garnet skarn, a distal green pyroxene–epidote skarn, and two quartz-rich varieties, a blue-green garnet skarn and light green pyroxene–garnet skarn, which occur as patches and small bodies within the former skarn types. The proximal massive brown garnet skarn zone is centered on two 060° trending faults in Mine 2, where the highest gold grades (5–10 g/t) were observed. It grades into a distal green pyroxene–epidote skarn zone to the North (Cuerpo 3). Granditic garnet shows iron enrichment from the proximal to the distal zone. Diopsidic pyroxene exhibits iron and manganese enrichment from proximal to distal zones. The retrograde stage is weakly developed and consists mainly of mineral phases filling centimeter-wide veins, vugs, and interstices between garnet and pyroxene grains. The main filling mineral is quartz, followed by K-feldspar, epidote, calcite, and chlorite, with minor sericite, apatite, titanite, hematite, pyrite, chalcopyrite, and gold. Metal and sulfur contents are low at Fortuna, and the highest gold grades coincide with high hematite abundance, which suggests that retrograde stage and gold deposition took place under oxidizing conditions. Fluid inclusions from pyroxene indicate precipitation from high temperature—high to moderate salinity fluids (400 to 460°C and 54- to 13-wt% eq. NaCl), which result probably from boiling of a moderately saline (~8-wt% eq. NaCl) magmatic fluid. Later cooler (180 to 475°C) and moderate to low saline fluids (1- to 20-wt% eq. NaCl) were trapped in garnet, epidote, and quartz, and are interpreted to be responsible for gold deposition. Chlorite analysis indicates temperature of formation between 300 and 340°C in accordance with fluid inclusion data. It appears, thus, that gold was transported as chloride complexes under oxidizing conditions and was deposited at temperatures around 300°C when transport of chloride complexes as gold carriers is not efficient.

Keywords Fortuna mine · Nambija district · Gold · Skarn · Zonation · Endoskarn

Editorial handling: D. Lentz

A. Markowski (✉) · J. Vallance · M. Chiaradia · L. Fontboté
Section des Sciences de la Terre, University of Geneva,
Rue des Maraîchers 13,
1205 Geneva, Switzerland
e-mail: markowski@erdw.ethz.ch

A. Markowski
Isotopengeologie und Mineralische Rohstoffe, ETH-Zentrum,
NW C81.1, Clausiusstrasse 25,
8092 Zürich, Switzerland

Introduction

Nambija, one of the most important gold districts in Ecuador, is located in the southern part of the country (Zamora province) in the Cordillera del Cóndor (sub-Andean zone) at elevations ranging from 1,600 to 2,300 m. The district includes, from north to south, the gold skarn deposits of Fortuna, Cambana, Campanillas, Nambija, Guaysimi, and Sultana del Cóndor (Paladines and Rosero 1996; Prodeminca 2000; Fontboté et al. 2004; Fig. 1). Cu–Au and Cu–Mo porphyries also occur in the district

(e.g., Cerro Colorado and Cumay, Fig. 1). The gold deposits of the area were exploited first by the Spanish conquerors during the 16th century (Prodeminca 2000), but they were subsequently abandoned. The rediscovery of the mineralization in the early 1980s led to a gold rush and extensive informal mining because of high gold grades up to several hundred g/t Au. In 1990, the total resources were estimated at 23 Mt at 15 g/t Au (Mining Magazine 1990). In 2000, this number was reevaluated at 125–155 t Au and the production was estimated at 60–90 t Au since 1980 (Prodeminca 2000).

Litherland et al. (1992, 1994) and Prodeminca (2000) proposed that skarn formation and gold mineralization are unrelated and that gold deposition took place "under epithermal conditions." Hammarstrom (1992) proposed a "gold-associated skarn" model in a reconnaissance study and Meinert (1998, 2000) classified Nambija as an "oxidized gold skarn" in a worldwide compilation of gold-bearing skarns. Fontboté et al. (2004), in an overview of the Nambija district, place gold deposition in the early retrograde phase of a skarn event related to Late Jurassic magmatism.

The present study on the Fortuna deposit, the northernmost gold skarn occurrence of the Nambija district, provides the first detailed description of a deposit in the district. Although the general skarn assemblages are the same as those described in Fontboté et al. (2004), Fortuna is, so far, the only deposit where clear zoning of the prograde and retrograde mineral assemblages and of the metal content at the deposit scale has been recognized, and this paper is particularly focused on this subject. We also provide the first description of the endoskarn observed at Fortuna and description of the porphyritic intrusion, which is believed to have formed the skarn. Our results support the hypothesis that the gold mineralization of Fortuna is related to the retrograde phase of the skarn, as proposed by Meinert (1998, 2000) and Fontboté et al. (2004).

Geological setting of the Nambija district

The Nambija region occurs in the Jurassic arc situated at the western margin of the Amazon craton and east of the oceanic and continental terranes accreted between Early

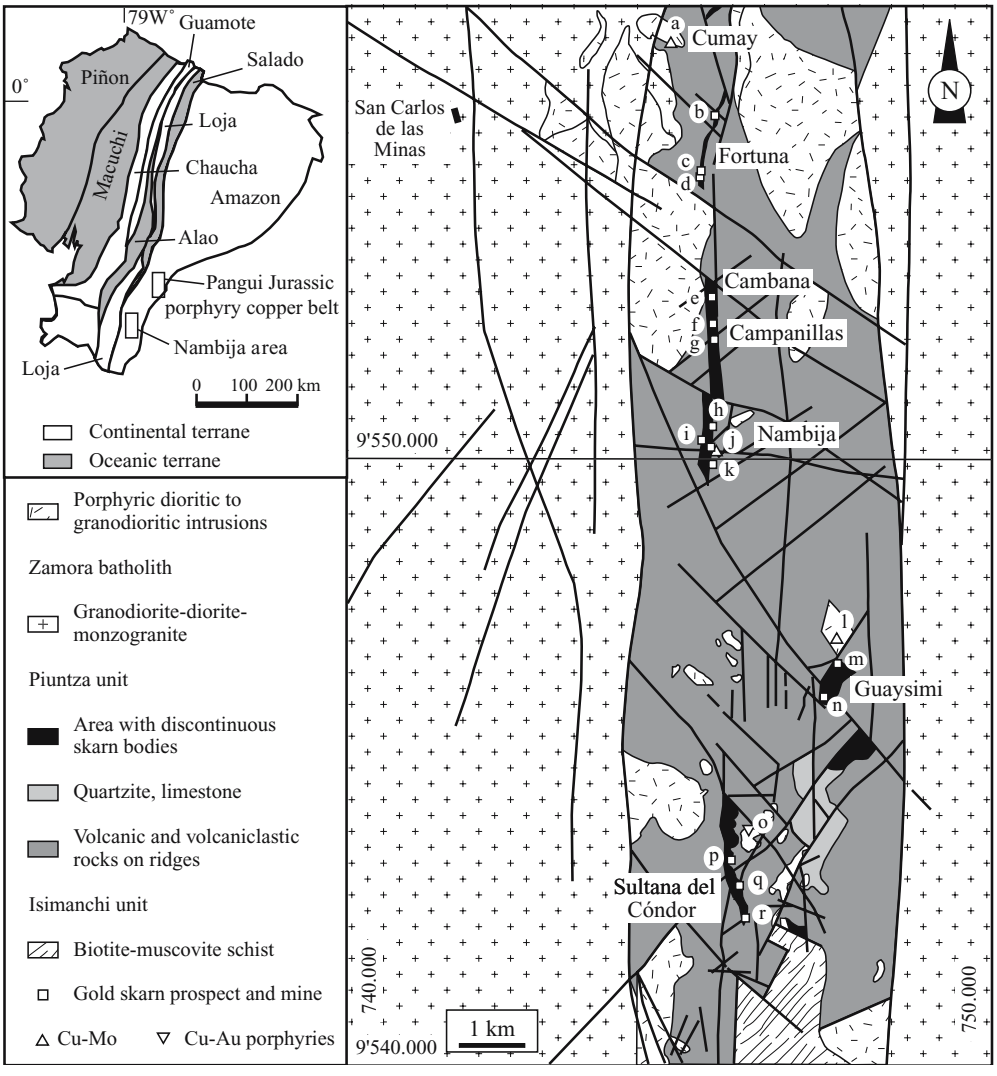

Fig. 1 Structural map of Ecuador (modified from Litherland et al. 1994) and simplified geologic map of the Nambija district (modified from Prodeminca 2000). **a** Cumay Cu–Mo porphyry (prospect), **b** Fortuna–Cuerpo 3 (prospect), **c** Fortuna–Mine 1 (abandoned workings), **d** Fortuna–Mine 2 and Southern Sector (open pit), **e** Cambana (open pit), **f** Campanillas–Katy (abandoned workings), **g** Campanillas main present workings (open pit and underground), **h** Nambija–El Arco (open pit and underground), **i** Nambija–El Playón–Mapasingue (underground), **j** Nambija–El Tierrero gold skarn and Cu–Mo porphyry (open pit and underground), **k** Nambija–El Diamante (prospect), **l** David Cu–Mo porphyry (prospect), **m** Guaysimi–Banderas (open pit), **n** Guaysimi–Central (open pit), **o** Cerro Colorado–Tumi Cu–Au porphyry (prospect), **p** Sultana del Cóndor–Bruce (open pit and underground), **q** Sultana del Cóndor–Central (open pit and underground), **r** Sultana del Cóndor–Toscón (open pit and underground)

Cretaceous and Eocene (Feininger 1987; Litherland et al. 1994; Jaillard et al. 1997; Hughes and Pilatasig 2002; Fig. 1). The geology of the Nambija district consists of 1) unexposed Precambrian migmatitic gneiss, recorded in boreholes and as rafts in the Zamora Jurassic batholith, and 2) carboniferous black and green phyllites and marbles (Isimanchi unit). Sedimentary units cover the basement and include the Triassic Piuntza unit, which is the direct host to the Nambija mineralization. The whole sequence is intruded by the Jurassic Zamora batholith and covered by the Misahuallí andesitic volcanic/volcaniclastic unit considered as co-magmatic with the Zamora batholith (Litherland et al. 1994).

Gold-bearing skarn bodies of the Nambija district are hosted by the Triassic Piuntza continental/marine volcano-sedimentary unit (Fig. 1), which was first described by Litherland et al. (1994). Subsequent field studies (Paladines and Rosero 1996; Prodeminca 2000; Fontboté et al. 2004; this work) provided more detailed stratigraphic data, but continuous stratigraphy is still not available as the Piuntza unit occurs as discontinuous outcrops preserved from erosion by skarnification. As a consequence of this structural landform and the lack of outcrops in the rainforest outside the area of mining interest, unaltered rocks of the Piuntza unit could not be observed.

In the Nambija district, the Piuntza unit lies unconformably on the Carboniferous Isimanchi unit to the south (Fig. 1) and is overlain by the Jurassic Misahuallí unit to the north. In the main part of the district, it occurs as a flat roof over the Zamora batholith and is limited to the west and the east by two NS faults (Prodeminca 2000). According to Paladines and Rosero (1996), the Piuntza unit has a minimum thickness of 500 m of which 300 m crop out at Nambija. According to Prodeminca (2000), the basal Piuntza unit, which crops out in the southern part of the district, consists of calcareous siltstone, calcareous shale, siltstone, black shale, andesitic to andesitic–basaltic fine- to coarse-grained volcaniclastic rocks, breccias, and lava flows. In places, grey siltstone and black shales form several-centimeters thick to tens of centimeters thick alternating levels, volcaniclastic rocks show sorting, and coarse-grained volcaniclastic rocks and breccias contain lithic fragments of both volcanic and nonvolcanic origin. The upper part of the Piuntza unit crops out at El Tierrero (Nambija) and mainly at Fortuna. It consists of andesitic to basaltic–andesitic fine-grained to coarse-grained volcaniclastic rocks and lava flow (Appendix, Table 1, Fig. 2). Coarse-grained volcaniclastic rocks contain lithic fragments of volcanic origin, like pumice, which show spherulitic, porphyritic, or trachytic texture in a matrix of finer grained fragment, broken feldspars, and glass shards. No carbonate rocks were recognized, but some discontinuous fine-grained unskarnified layers containing bioclasts were observed in the Fortuna mine (see below).

The volcanic fraction is more important in the upper part of the Piuntza unit than in the basal part and causes an increase of the volcanic component to the north, as previously suggested by Litherland et al. (1994). As the Misahuallí unit is essentially made of andesitic volcanic/volcaniclastic rocks, distinction between the latter and the upper part of the Piuntza unit could be difficult. Lamprophyres, dikes, and sills, in places skarnified, cut the Piuntza unit (Appendix). They were not observed in the later Zamora batholith and porphyritic felsic intrusions.

In the Nambija district, bedding strikes dominantly east ±20° with dips of 10 to 50° S. At Nambija, the Piuntza unit forms an east-trending syncline. The Triassic age of the Piuntza unit is based on bivalve fossils encountered in skarnified rocks at Guaysimi and identified as *Costatoria* of Middle-Upper Triassic age (Woods and Morris 1992 in Litherland et al. 1994). The Piuntza unit is not found farther north in Ecuador, which suggests that it was deposited in a restricted basin (Litherland et al. 1994).

The Zamora batholith consists of equigranular fine-grained to coarse-grained I-type tonalite and granodiorite (Salazar E, unpublished report; Litherland et al. 1994). Litherland et al. (1994) applied whole rock Rb/Sr dating to four groups of samples from the Zamora batholiths and obtained ages of 187±2 Ma (five samples), 198±34 Ma (six samples), 246±17 Ma (six samples), and 144±35 Ma (five samples). They interpreted the first (187±2 Ma) as the most likely age of emplacement. Litherland et al. (1994) also dated hornblende and biotite from various localities and lithologies of the Zamora batholith. The 29 K–Ar ages

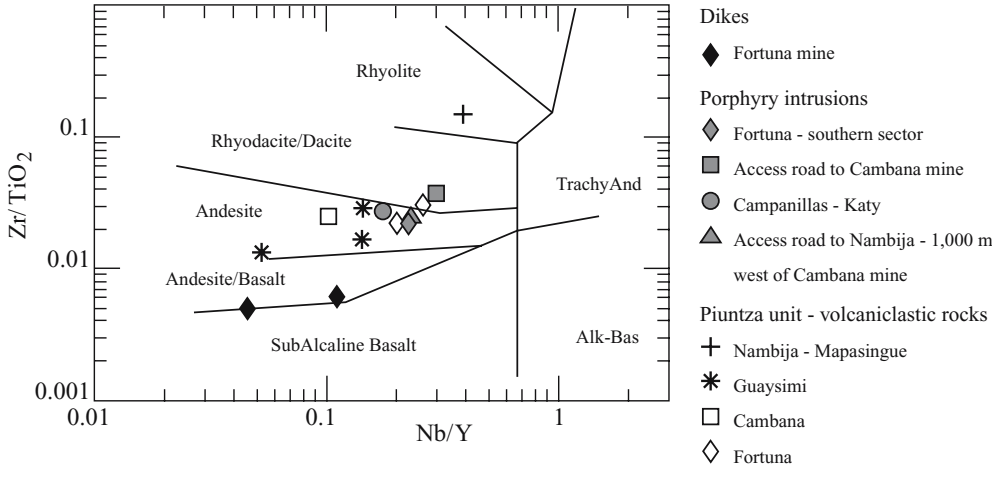

Fig. 2 Porphyry intrusions and volcanic and volcaniclastic rocks belonging to the Piuntza unit from Fortuna, Cambana, Campanillas, Nambija, Guaysimi plotted in a Zr/TiO_2 vs Nb/Y diagram (Winchester and Floyd 1976). Major and trace compositional data of these rocks are listed in Appendix

Table 1 Representative compositions of different type of skarns, volcaniclastic rocks and intrusion of Fortuna mine

Sample	DTR214	DTR215	DTR175	DTR179	DTR132	DTR195	DTR207	DTR210	DTR194	DTR227	DTR156	DTR184	DTR221
Location	Cuerpo 3		Mine 1		Mine 2		Southern Sector		Mine 2		Southern Sector		Mine 1
Coordinates	745.665/9′ 554.825	745.555/9′ 555.000	745.739/9′ 554.250	745.743/9′ 554.312	745.746/9′ 554.146	745.765/9′ 554.125	745.728/9′ 554.015	745.718/9′ 554.014	745.769/9′ 554.154	745.744/9′ 554.155	745.687/9′ 554.011	745.444/9′ 554.018	745.746/9′ 554.330
									← Increasing skarnification–decreasing Na_2O –				
Description	Brown and blue-green garnet skarn	Green pyroxene–epidote skarn	Green pyroxene–epidote skarn	Brown garnet skarn with retrograde alteration	Brown and blue-green garnet skarn	Blue-green garnet skarn ± brown garnet skarn	Blue-green garnet skarn	Brown garnet skarn	Skarnified tuff (40% pyroxene+ actinolite)	Weakly skarnified tuff (10% pyroxene+ actinolite)	Na-metasomatized tuff (1–2% pyroxene)+K-alteration along veins	Quartz–diorite porphyry	Dike
SiO_2	40.89	42.52	45.88	38.41	43.66	48.83	41.96	41.11	62.69	55.98	62.37	63.45	44.70
TiO_2	0.12	0.59	0.70	0.34	0.24	0.32	0.10	0.20	0.35	0.64	0.48	0.41	0.86
Al_2O_3	4.97	12.81	16.23	10.69	10.61	8.61	7.46	8.46	11.60	17.28	16.22	17.29	15.26
Fe_2O_3	21.94	13.04	12.45	12.03	12.59	13.79	19.15	18.60	5.31	5.85	4.98	4.25	9.72
MnO	1.25	1.65	0.72	1.18	1.64	1.09	1.13	1.29	0.39	0.30	0.05	0.14	0.76
MgO	0.15	3.38	1.40	4.04	0.48	0.34	0.65	0.22	0.10	3.22	0.87	1.14	8.56
CaO	29.44	23.68	19.61	23.53	29.33	25.30	27.42	28.14	13.90	5.55	1.26	4.53	10.22
Na_2O	n.d.	n.d.	n.d.	0.16	n.d.	n.d.	n.d.	0.47	0.07	3.49	4.86	3.71	2.26
K_2O	0.01	0.02	0.03	1.19	0.03	0.08	1.11	0.25	4.67	4.60	5.04	2.93	1.84
P_2O_5	0.05	0.28	0.13	0.23	0.18	0.53	0.07	0.06	0.20	0.27	0.09	0.17	0.16
LOI	0.10	0.10	2.46	7.40	0.87	0.09	0.02	0.01	0.02	2.12	2.80	1.32	4.81
Total	98.92	98.05	99.62	99.21	99.61	98.97	99.07	98.80	99.29	99.31	99.02	99.34	99.15
Pb[a]	25	17	17	15	18	22	23	24	12	10	11	5	14
Zn[a]	239	83	39	86	23	42	32	23	12	56	23	35	237
Cu[a]	59	145	20	37	14	25	140	56	9	26	1,440	17	130
Ni[a]	0	8	5	7	3	7	5	3	0	6	3	2	43
Co[a]	66	46	68	36	51	54	53	64	71	67	30	46	37
Cr[a]	5	34	37	57	13	25	22	21	26	15	12	8	158
S[a]	175	1,224	559	1,369	9	0.1	17	6,081	0	6,422	9,273	0	1,727
As[a]	53	5	6	4	9	13	31	24	9	7	5	7	8
Au[b]	27	28	>5,000	1,270	3.87	33	214	25	69	n.a.	22	7	109
Mo[c]	<5	<5	<5	<5	<5	<5	<5	5	<5	n.a.	<5	<5	<5
Ag[c]	8	<5	<5	<5	<5	<5	<5	7	<5	n.a.	<5	<5	<5
Sb[c]	0.3	3.1	4.8	0.9	0.3	0.8	1.2	<0.2	0.5	n.a.	0.6	0.6	2.4

Table 1 (continued)

Sample	DTR214	DTR215	DTR175	DTR179	DTR132	DTR195	DTR207	DTR210	DTR194	DTR227	DTR156	DTR184	DTR221
Location	Cuerpo 3		Mine 1		Mine 2		Southern Sector		Mine 2		Southern Sector		Mine 1
Coordinates	745.665/9′	745.555/9′	745.739/9′	745.743/9′	745.746/9′	745.765/9′	745.728/9′	745.718/9′	745.769/9′	745.744/9′	745.687/9′	745.444/9′	745.746/9′
	554.825	555.000	554.250	554.312	554.146	554.125	554.015	554.014	554.154	554.155	554.011	554.018	554.330
							← Increasing skarnification–decreasing Na_2O						
Hg[c]	1	<1	2	<1	3	3	3	2	2	n.a.	<1	1	<1
Bi[d]	1.2	0.9	1	<0.5	<0.5	<0.5	0.6	n.a.	n.a.	n.a.	n.a.	n.a.	n.a.
Te[d]	0.8	<0.5	0.6	<0.5	<0.5	0.5	0.5	n.a	n.a.	n.a.	n.a.	n.a.	n.a.

All samples except DTR 221 are ordered from north to south. Major element oxides are reported in wt%, Cr_2O_3 below detection limit; trace elements are reported in ppm but Au in ppb
n.a. Not analysed, *n.d.* not detected, *LOI* loss on ignition
[a]Data collected by XRF
[b]Gold abundance were collected by fire assay and atomic absorption methods and are measured in parts per billion (ppb)
[c]Data collected by neutron activation
[d]Data collected by atomic absorption

obtained ranged from 140 to 190 Ma with a mode between 170 and 190 Ma, which they interpreted as the intrusion of the main phase of the batholith, whereas, the youngest ages probably reflect later resetting.

The Piuntza unit and the Zamora batholith are cut by several porphyritic intrusions all extensively hydrothermally altered with K- and/or Na-metasomatism (Figs. 1, 2, and 3). Syenite porphyries were described by McKelvey and Hammarstrom (1991) and Hammarstrom (1992) based on modal mineralogy. Paladines and Rosero (1996) described "quartz–feldspar porphyries" in which mineral abundance indicates dioritic, granodioritic, and monzodioritic compositions. Because of extensive alkali metasomatism and weathering, only immobile elements and petrographic observation (including relictic minerals and phantom textures) could be used to assess each intrusion's composition. Immobile element data from Campanillas, Cambana, and Fortuna samples suggest mainly quartz–dioritic to granodioritic compositions (Fig. 2, Table 1, Appendix) in agreement with modal mineralogy. According to tectonic environment discrimination diagrams of Pearce et al. (1984), the porphyries have a volcanic arc signature (Markowski 2003). A K–Ar age of 141±5 Ma was obtained by Prodeminca (2000) on hornblende from the quartz–monzonite porphyry intrusion related to the Cu–Mo mineralization of the Cumay prospect 1-km north of Fortuna (Fig. 1). This age is slightly younger than K–Ar ages of 154± 5 Ma (whole rock) and 157±5 Ma (hornblende) obtained from the Pangui porphyry copper intrusions within the Zamora batholith, 70 km to the north of the Nambija district (Gendall et al. 2000; Prodeminca 2000). The 141±5-Ma age of the Cumay porphyry (belonging to the Nambija district) is, within error, the same as two Re–Os ages (145.92±0.46 and 145.58±0.45 Ma) reported by Fontboté et al. (2004) on two molybdenite samples from post skarn sulfide-rich veins of the Nambija–El Tierrero Cu–Mo prospect (Fig. 1). K–Ar determinations on K-feldspar and sericite from mineralized veins (Prodeminca 2000) yield younger ages, of 102±3 Ma (Cumay Cu–Mo prospect) and 100±3 and 116±4 Ma (Nambija–El Tierrero Cu–Mo prospect, Fig. 1), which probably reflect later resetting already invoked by Litherland et al. (1994) for the Zamora batholith.

Prodeminca (2000, p. 181) identified three main sets of structures in the Nambija district (Fig. 1). The first constitute north–south dextral reverse fractures, which limit the district both east and west, and by coeval northeast-striking, steeply dipping fractures with, locally, sinistral displacement. The main gold mineralization is controlled by the northeast-striking fractures, in part, as tensional veins. A second set consists of northwest-striking reverse faults and thrust planes dipping 10 to 40° SW, which cut the previously mineralized structures. All these structures are crosscut by a third set of east-striking steeply dipping normal dextral faults.

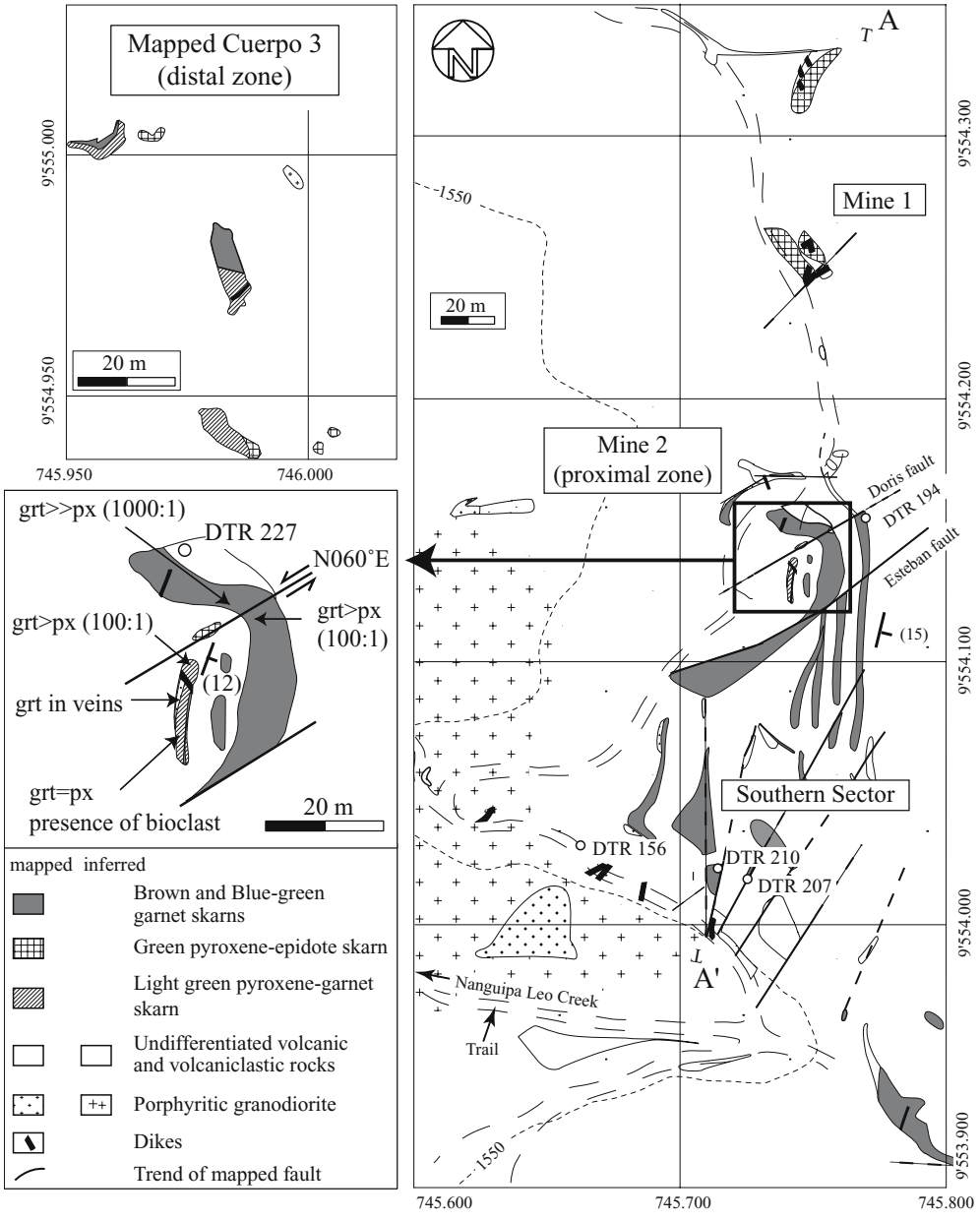

Fig. 3 Geological map of the Fortuna mine showing the four mineralized areas, which are, from north to south: Cuerpo 3, Mine1, Mine 2, and Southern Sector. Cuerpo 3 is shown separately as it outcrops about 1-km north of other sites. The highest gold grades were observed in Mine 2 between the Doris and Esteban faults and both are closely related to the skarn formation. Mine 2 is interpreted as the proximal zone, whereas, Cuerpo 3 is the distal one. Location of samples DTR 156, DTR 194, DTR 207, DTR 210, and DTR 227 are displayed on the geological map. Chemical compositions of these samples are reported in Table 1

Analytical methods

Two field campaigns of 4 and 2 weeks, respectively, were carried out during February–March 2002 and June 2003. A detailed 1:400 scale geological map of parts of the Fortuna mine was produced and a simplified version is shown in Fig. 3. Three hundred and fourteen samples of igneous rocks, skarn, and mineralization samples from Fortuna and other parts of the district (Cambana, Campanillas, and Guaysimi) were collected.

Petrographic studies were carried out on hand specimen slabs followed by a study of about 150 thin and polished sections under the microscope. Microprobe analyses were performed on garnet, pyroxene, epidote, amphibole, chlorite, and gold of selected samples. The analyses were carried out at the Institute of Mineralogy and Geochemistry of Lausanne (Switzerland) on a Cameca Camebax SX 50 electron microprobe. The beam current and voltage have been adapted to each mineral analyzed as following: 20-nA current and a 15-kV acceleration voltage for garnet, 15-nA current and a 15-kV acceleration voltage for epidote, 10-nA current and a 15-kV acceleration voltage for amphibole, 10-nA current and a 15-kV acceleration voltage for chlorite, 15-nA current and a 15-kV acceleration voltage for pyroxene and gold was analyzed using a 50-nA current and a 15-kV acceleration voltage. Gold grains were analyzed for Au, Ag, S, As, Hg, Bi, Te using native gold, native silver, pyrite, GaAsSb, cinnabar, and BiTe standards.

Major and trace elements were measured by X-ray fluorescence (XRF), using fused and pressed pellets, respectively. XRF analyses of 31 skarn rocks, seven volcanic/volcaniclastic rocks, two dikes, and four intrusive rock samples were performed at the Centre d'Analyses

Minérales (CAM) of the Lausanne University on a Philips PW 2400 XRF machine. Additional trace elements (e.g., Au, Ag, Hg) and rare earth elements (REE) were analyzed by Instrumental Neutron activation by the XRAL, Ontario (Canada), with a detection limit for gold of 5 ppb. Gold values higher than 5,000 ppb were analyzed by fire assay with gravimetric finish. Bismuth and tellurium were analyzed by Na_2O_2 fusion and hybrid atomic absorption at the same laboratory. Because of the limited size of the analyzed sample, the metal abundances are not the same as grades and cannot be considered in economic terms.

Heating and freezing analyses of fluid inclusions were obtained on ~100-μm thick, doubly polished rock sections. A Linkam THMSG600 heating and freezing stage mounted on a DMLB Leica microscope equipped with a Nikon ×100 long working distance lens was used for microthermometric measurement, as described by Shepherd (1981). The system was calibrated with synthetic fluid inclusions at −56.6, 0.0, and 374.1°C (Sterner and Bodnar 1984). Low-temperature measurements have an uncertainty of ±0.1°C, whereas, high-temperature measurements have a precision of ±1°C. Salinities were calculated in the NaCl–H_2O system from final ice melting temperature between 0.0 and −21.1°C, using equations published in Bodnar and Vityk (1994). In the case of halite- (±sylvite-) bearing inclusions, salinities were calculated by the melting temperature of the solid(s) using the equation of Sterner et al. (1988) and the computer program AqSo1e of Bakker and Brown (2003).

Local geology of the Fortuna mine

Four mineralized sites, all hosted by garnet–pyroxene skarn, have been studied at Fortuna during the present study. From north to south they are: Cuerpo 3, Mine 1, Mine 2 and the Southern Sector (Figs. 3 and 4). In the past, quartz–K–feldspar veins were mined at Mine 1, with gold grades ranging between 5 and 8 g/t (J. Escobar, oral communication 2001). Mine 2 is the currently mined site, with gold grades reaching up to 10 g/t, the highest grades being bounded between two major 060°-trending faults (Doris and Esteban faults; Figs. 3 and 4). The northernmost sector (Cuerpo 3) and the Southern Sector are not economic. A quartz–diorite porphyritic intrusion (Figs. 2, 5g, and 6a; sample DTR184 in Table 1) crops out in the Southern Sector. This intrusion is the only one known in the Nambija district with exposure fresh enough to determine the original composition and petrography. Up to 5-mm zoned euhedral plagioclase represents 50–60 vol% of the rock. Rounded quartz phenocrysts up to 7 mm represent 5–10 vol% of the rock and K-feldspar phenocrysts up to 10 vol%. Hornblende is the only mafic mineral forming euhedral phenocrysts up to 7 mm with an abundance of 5–10 vol%. The groundmass represents 20 to 40 vol% in volume and is composed of an equigranular mixture of fine-grained (<300 μm) K-feldspar and subrounded quartz. Accessory minerals are zircon and apatite. All observed samples show at least one stage of hydrothermal alteration (K-silicate alteration, endoskarn, sericitic alteration, see below).

Bedding of the Piuntza volcaniclastic rocks strikes at Fortuna N 020° E and dips 10 to 15° E. The existence of minor amounts of intercalated calcareous-rich sedimentary rocks is inferred from the observations of bioclast relicts within unskarnified whitish layers in Mine 2 (Fig. 3). These whitish layers occur as intercalation within the light green pyroxene–garnet skarn and brown garnet skarn that crop out between the Doris and the Esteban faults in Mine 2 (Fig. 3).

Faults in Mine 1 and Mine 2 revealed three preferential orientations, which are similar to those described at the district scale. The main direction is NE–SW, dipping about

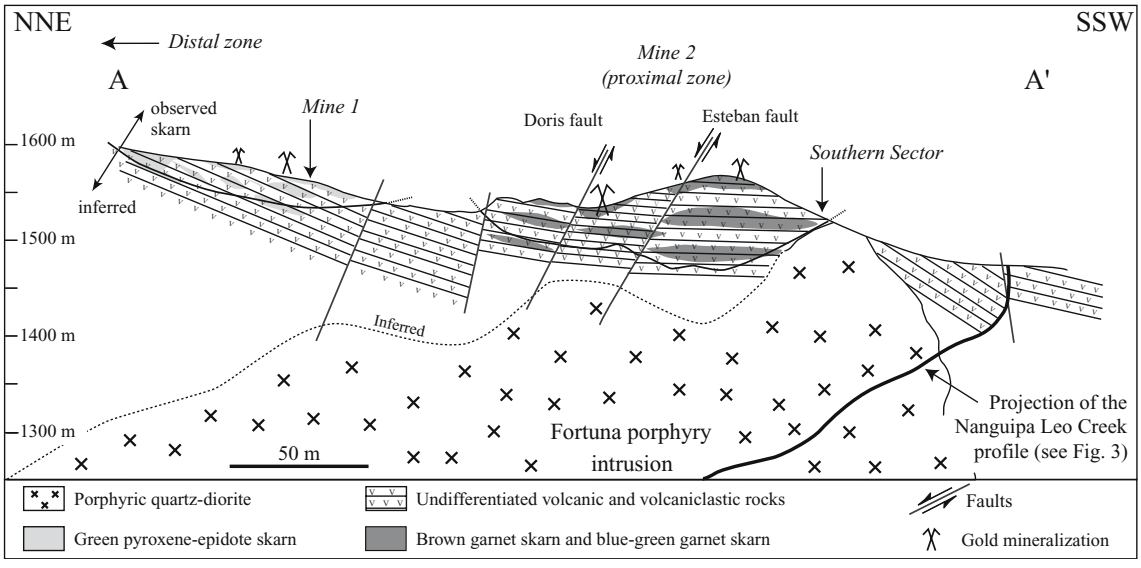

Fig. 4 Schematic cross-section of the Fortuna mine from Mine 1 to the Southern Sector, illustrating the close spatial relationship of the skarn and the Fortuna quartz–diorite porphyritic intrusion. This section was drawn based on information from the surface mapping and observation along the Nanguipa Leo Creek

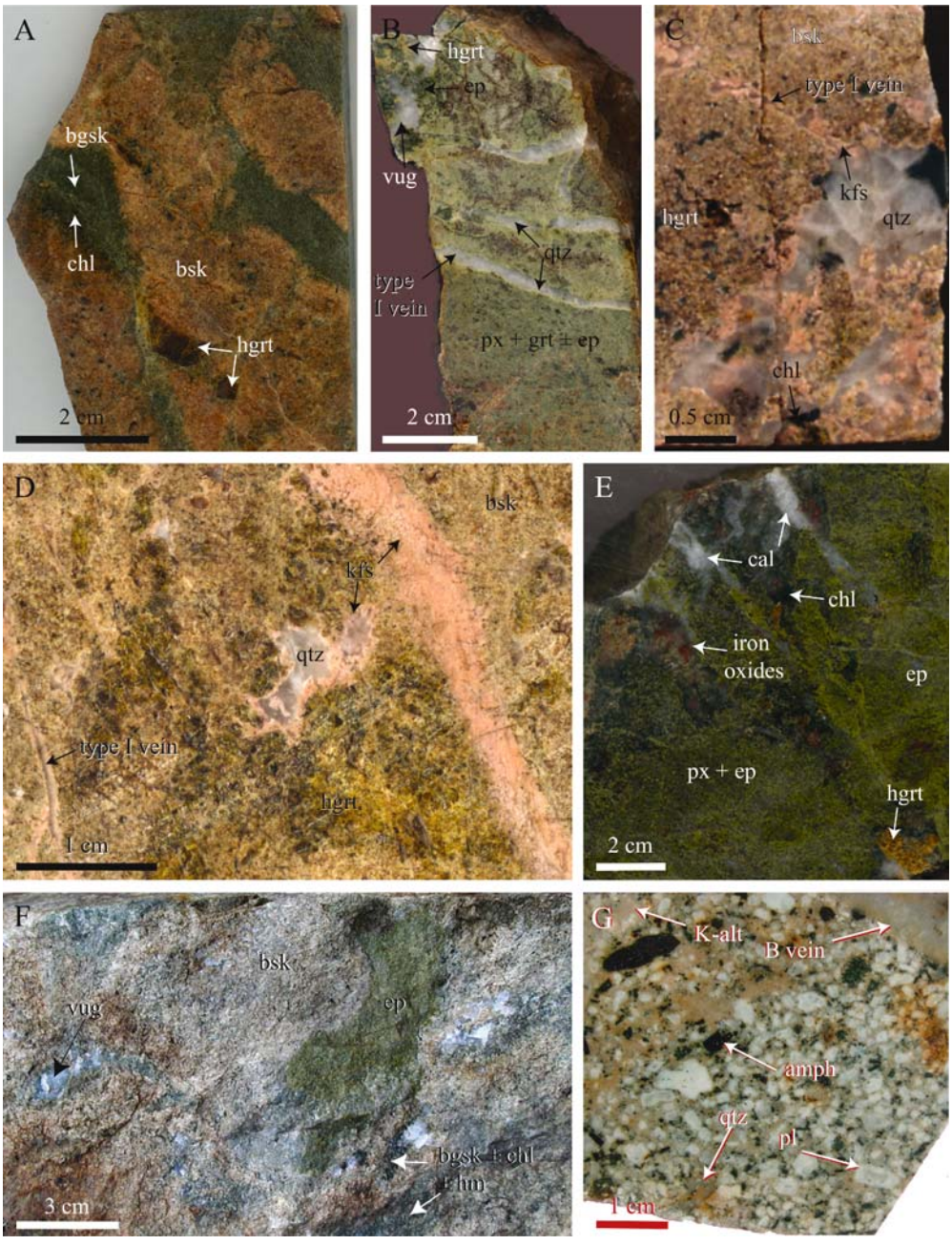

Fig. 5 Photographs of selected samples from the Fortuna mine. **a** Layers of *blue-green* garnet skarn (*bgsk*) in the *brown* garnet skarn (*bsk*). Clusters of *dark honey-reddish* garnet (*hgrt*) occur in the latter. Sample DTR 132, Mine 2. **b** *Green* pyroxene–garnet skarn (px+grt±ep) with a vug filled with quartz (*qtz*), epidote (*ep*) and *dark honey-reddish* garnet and several type I quartz veins. Sample DTR 135, Cuerpo 3. **c**–**d** *Brown* garnet skarn, *dark honey-reddish* garnet. Vugs and type I veins are filled with quartz, K-feldspar (*kfs*), and chlorite (*chl*). Sample DTR 208, Southern Sector. **e***Green* pyroxene–epidote skarn (*ep* + *px*) and vugs filled with *dark honey-reddish* garnet, calcite (*cal*), chlorite, and iron oxides. Chlorite and iron oxides are dominant in the darker areas. Sample DTR 129, Mine 1. **f** Lenses of *green* pyroxene–epidote skarn in the *brown* garnet skarn in Mine 2. The *brown* garnet skarn shows a transition to *blue-green* garnet skarn and vug. The *blue-green* garnet skarn shows visible retrograde alteration into chlorite and hematite (*hm*). **g** Sample of the Fortuna quartz–diorite porphyritic intrusion cropping out in the Southern Sector, showing euhedral amphibole (*amph*), subhedral plagioclase (*pl*), rounded quartz phenocrysts and potassic alteration (*K-alt*). A quartz ± pyrite ± K-feldspar B vein crosscuts the whole. Sample DTR 184

40° to the SE; a second direction is represented by almost N–S (±30°) trending faults with subvertical dipping. A subordinate system of faults have, in general, NE–SW to E–W orientation and dip 90 to 60° NW.

Skarn mineralogy and zoning at the Fortuna mine

At the mine scale, the geometry of the skarn bodies, which form 30 cm up to 3-m thick massive layers in a ≥70-m thick portion of the Piuntza unit, is largely controlled by bedding and subordinately by the intersection of NE–SW fractures (Figs. 3 and 4). Massive skarn bodies are separated by less altered lithologies and mainly result from the complete replacement of volcaniclastic and volcanic rocks, and perhaps, of minor enclosed limestone and/or carbonate-rich volcaniclastic lenses.

The prograde-stage mineral phases are mainly garnet and pyroxene (Fig. 7). The retrograde stage is weakly developed and consists essentially of epidote, chlorite, calcite, hematite, and quartz replacing the prograde mineral assemblage. These retrograde minerals fill also centimeter-wide veins and vugs together with K-feldspar and minor plagioclase, sericite, apatite, gold, pyrite, sphalerite, and chalcopyrite. Quartz, epidote, K-feldspar, and plagioclase generally occur slightly earlier than calcite, chlorite, sericite, apatite, gold, hematite, pyrite, sphalerite, and chalcopyrite (Fig. 7). Late retrograde sulfide-rich cross-cutting veins commonly observed in other parts of the Nambija district (Fontboté et al. 2004) are almost

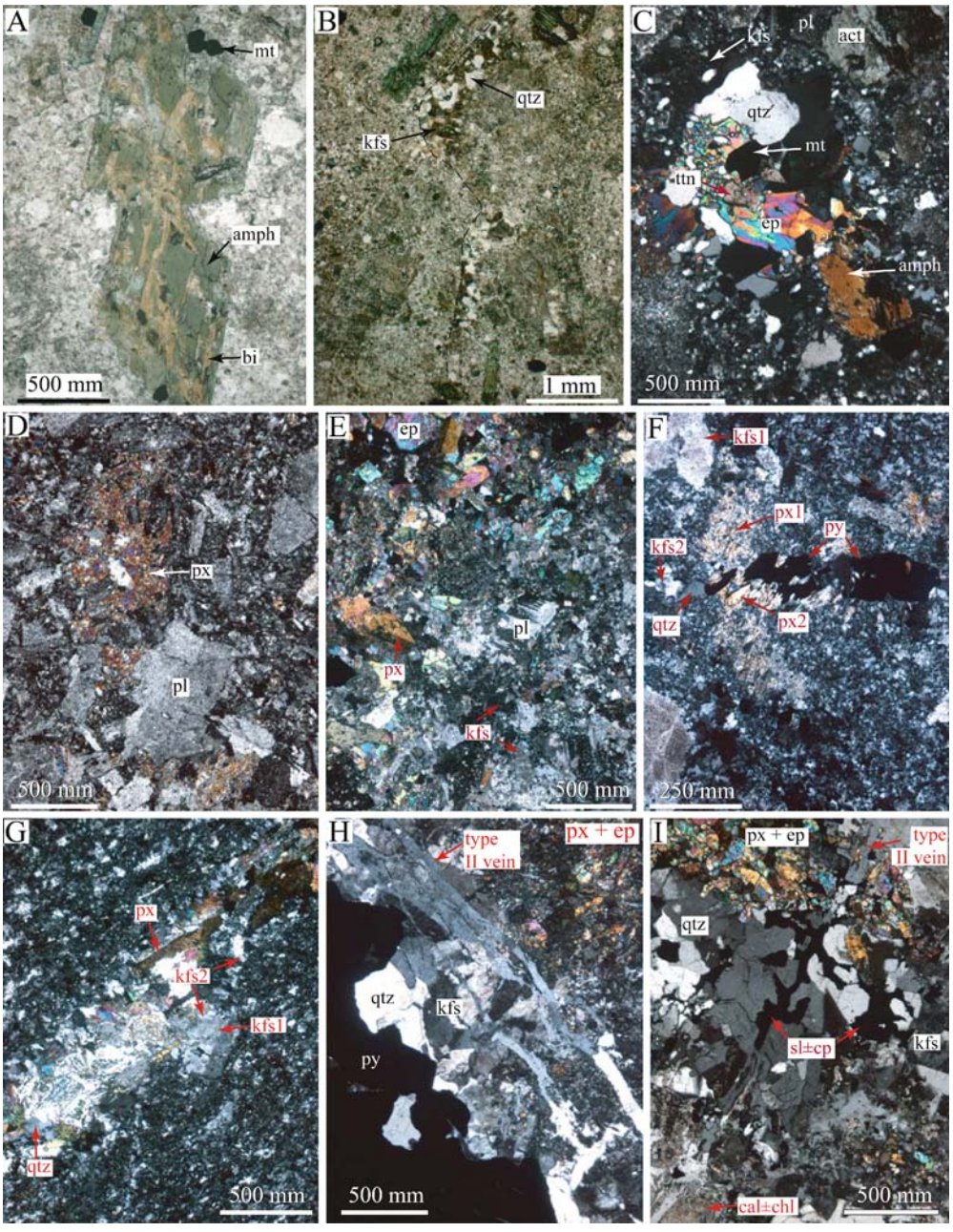

Fig. 6 Photomicrographs of rock alteration and veins at Fortuna. **a** Potassic alteration in the quartz-diorite intrusion. Amphibole (*amph*) is partially replaced by biotite (*bi*) and magnetite (*mt*). Sample DTR 184, Southern Sector. Transmitted light, parallel polar. **b** Discontinuous vugs filled with equigranular quartz (*qtz*) and K-feldspar (*kfs*) in the quartz–diorite intrusion. Sample DTR 184, Southern Sector. Transmitted light, parallel polar. **c** Endoskarn formation in the quartz–diorite intrusion with vug filled with quartz (*qtz*), Na-rich plagioclase (*pl*), epidote (*ep*), actinolite (*act*), magnetite (*mt*), titanite (*ttn*) ± K-feldspar (*kfs*). Sample DTR 184, Southern Sector. Transmitted light, crossed polar. **d** Alteration in the volcaniclastic rocks. Na-rich plagioclase, pyroxene (*px*) ± K-feldspar tend to obliterate the original fabric. Sample DTR 209, Southern Sector. Transmitted light, crossed polar. **e** Transition from altered volcaniclastic rock (*lower right*) to *green* pyroxene–epidote skarn (*upper left*) skarn front showing a band of K-feldspar and Na-rich plagioclase that obliterate the volcaniclastic texture. Sample DTR 61, Mine 1. Transmitted light, crossed polar. **f** Quartz, K-feldspar (*kfs1*) >> Na-rich plagioclase, pyroxene (*px2*), pyrite (*py*) ± chalcopyrite vein in the altered volcaniclastic rocks. K-feldspar and pyroxene in the vein are epitaxial when cutting K-feldspar (*kfs1*) and pyroxene (*px1*) from the altered volcaniclastic rocks. Sample DTR 156, Southern Sector. Transmitted light, crossed polar. **g** Quartz >> K-feldspar, pyroxene vein cutting a silty volcaniclastic rock. Sample DTR 194, Mine 2. Transmitted light, crossed polar. **h** Type II quartz vein cutting a vug filled with quartz, K-feldspar and pyrite. K-feldspar is sliced and quartz from the veins and vug are in optical continuity. Sample DTR 64a, Mine 1. Transmitted light, crossed polar. **i** Type II quartz, sphalerite (*sl*), and chalcopyrite (*cp*) vein crosscutting *green* pyroxene–epidote skarn (*px* + *ep*) and a vug filled with retrograde quartz, K-feldspar, calcite and chlorite (*cal±chl*). Sample DTR 64a, Mine 1. Transmitted light, crossed polar

nonexistent at Fortuna. Veins and vugs are hosted by massive skarn and sometimes extend up to several centimeters away from the skarn front.

Variable proportions of prograde minerals allow us to recognize a proximal and volumetrically dominant *massive brown garnet skarn, a distal green pyroxene-epidote skarn*, and two quartz-rich varieties, a *blue-green garnet skarn* and *a light green pyroxene-garnet skarn* (Figs. 3 and 4), which occur as patches and small bodies within the former skarn types.

The massive brown garnet skarn (Figs. 5a,c,d,f and 8e,g) is made up almost exclusively of ~1-mm isotropic to strongly zoned garnet with granditic to andraditic compositions (mean: Ad_{68}, range: $Ad_{24–98}$, Table 2 and Fig. 9). The isotropic garnet has compositions close to pure andradite. This skarn type is dominant in Mine 2 and Southern Sector; a large outcrop has been found in Cuerpo 3 (Figs. 3 and 4).

Green pyroxene-epidote skarn bodies (Figs. 5e,f and 8c) were recognized mainly at Mine 1 and Cuerpo 3 and occupy a distal position relative to the brown skarn at the deposit and outcrop scales. The skarn consists of subhedral to anhedral pyroxene grains, which are small (<150 μm) at Mine 1 and can reach up to 800 μm in length at Cuerpo 3, where it is also more abundant. Epidote ($Ps_{9.8–17.7}$) is particularly abundant in Mine 1 where it forms 100- to 500-μm euhedral grains; at Cuerpo 3, it is finer grained.

The blue-green garnet skarn typically occurs as irregular patches within the brown garnet skarn (Figs. 5a and f), mainly in Mine 2. It consists of strongly anisotropic garnet (mean: Ad_{62}, range: $Ad_{9–99}$, Table 2 and Fig. 9) with minor pyroxene and epidote within a quartz matrix (Figs. 5a,f and 8a,h). Garnet is mostly euhedral. In places, garnet grains are fractured in situ and cemented by coarse-grained quartz (Fig. 8a). Epidote and/or K-feldspar may replace garnet (Fig. 8b). The bluish color of this skarn is imparted by the quartz matrix (up to 50% volume), whereas, the greenish color is due to epidote and/or pyroxene. The transition between brown garnet skarn and blue-green garnet skarn is sharp, in part marked by chlorite (Fig. 5a), to gradational (Fig. 5f). The blue-green garnet skarn shows gradational contacts to the vugs filled with the retrograde assemblage quartz, K-feldspar and chlorite, calcite, pyrite, hematite, and gold (Fig. 5f).

The light green pyroxene–garnet skarn is a pyroxene-rich variety of blue-green garnet skarn, which occurs as patches within green pyroxene–epidote skarn, mainly close to the contact with brown garnet skarn (Fig. 3). It consists of pyroxene, anisotropic garnet, and minor epidote in a matrix of anhedral quartz grains up to 5 mm in size (Figs. 5b, 8d). Pyroxene ($Hd_{20–42}$, $Di_{46–67}$, $Jo_{9–14}$ in Cuerpo 3 and $Hd_{27}Di_{63}Jo_{10}$ in Mine 2, Fig. 9) occurs as subhedral to euhedral up to 2-mm long grains or up to 7-mm aggregates. Garnet is fractured without displacement and/or rotation of the fragments. The most grossular-rich compositions at Fortuna were found in this skarn variety (mean: Ad_{36}, Fig. 9; values at Mine 2, $Ad_{9–57}$; at Cuerpo 3, $Ad_{39–57}$). Epidote crystallization appears to be universally coeval with quartz as it occurs both as a replacement of

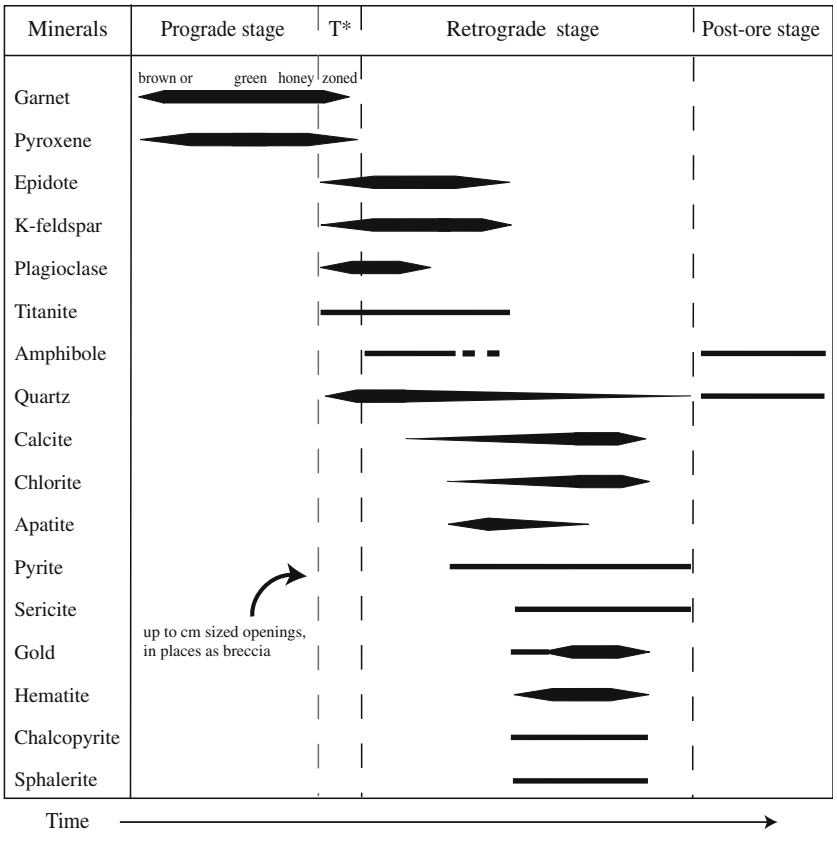

Fig. 7 Schematic paragenetic chart of the Fortuna gold skarn. *T** means a transition period, where time relationship between the different minerals are not clear or may be contradictory from one zone to other. Late retrograde sulfide-rich crosscutting veins commonly observed in other parts of the Nambija district (Fontboté et al. 2004) are almost nonexistent at Fortuna

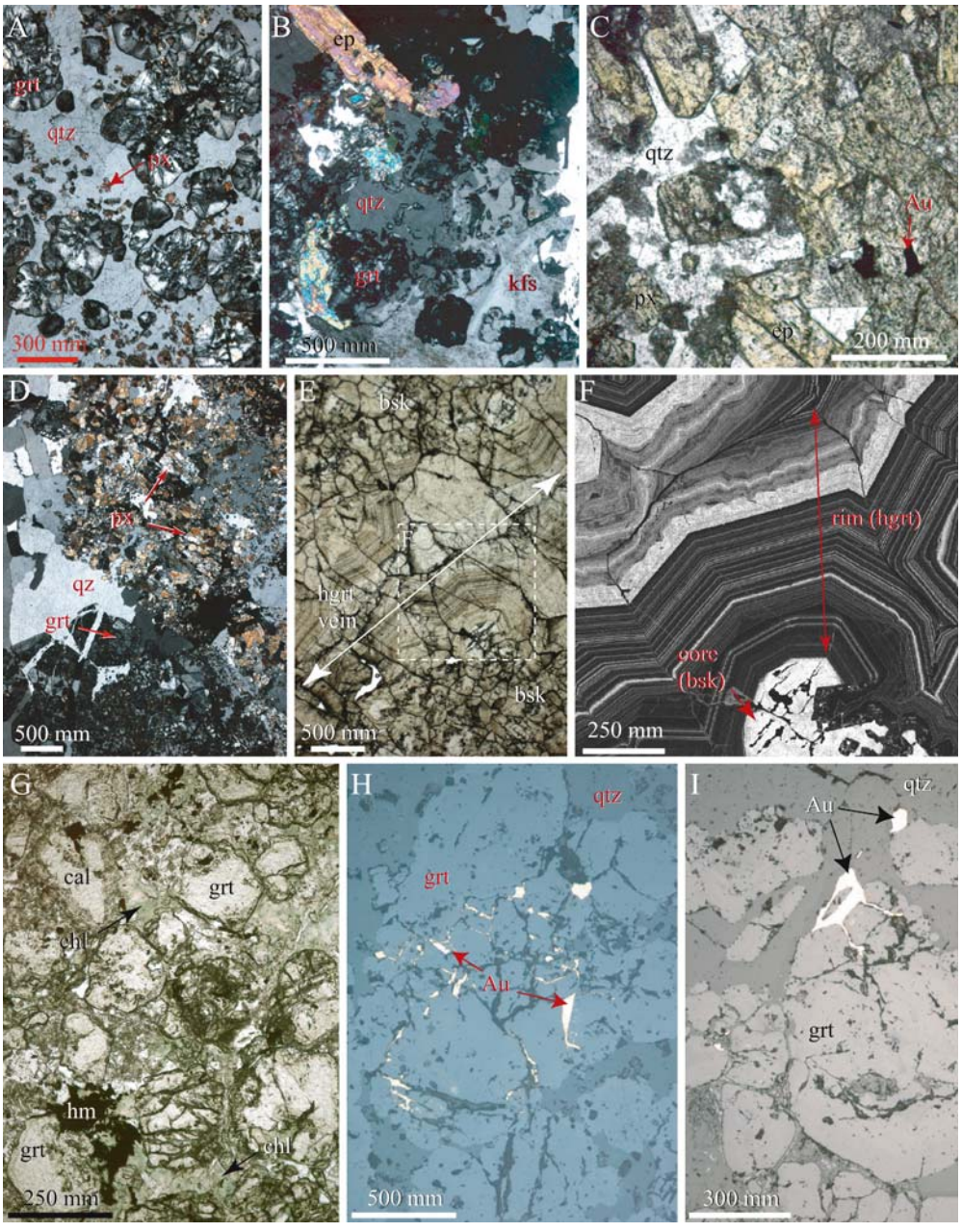

Fig. 8 Photomicrographs of selected samples from the Fortuna mine. **a** *Blue-green* garnet skarn with quartz (*qtz*) in apparent equilibrium with garnet (*grt*), subordinate pyroxene (*px*). Sample DTR 132, Mine 2. Transmitted light, crossed polar. **b** Epidote (*ep*) and K-feldspar (*kfs*) replacing garnet in the *blue-green* garnet skarn. Sample DTR 194, Mine 2. Transmitted light, crossed polar. **c** *Green* pyroxene–epidote skarn (*right*) grading to quartz–epidote vug to the left. Gold (*Au*) occurs between epidote grains. Sample DTR 175, Mine 1. Transmitted light, parallel polar. **d** Green pyroxene–garnet skarn at Cuerpo 3. Sample DTR 135. Transmitted light, crossed polar. **e** Vein of strongly zoned *dark honey-reddish* garnet (*hgrt*) cutting *brown* garnet skarn (*bsk*). *Box* locates photo. **f** Sample DTR 55, Mine 2. Transmitted light, parallel polar. **f** *BSE* image showing Al distribution in *brown* skarn garnet core and *dark honey-reddish* garnet rim. Light areas correspond to grossularitic garnet. Sample DTR 55, Mine 2. **g** Strongest retrograde alteration observed at Fortuna. The prograde assemblage (i.e., garnet) is replaced by chlorite (*chl*), calcite (*cal*), and hematite (*hm*), but the type of skarn is still recognizable (here, *brown* garnet skarn). Sample DTR 132, Mine 2. Transmitted light, crossed polar. **h** Gold occurring in fractured garnet of the *blue-green* garnet skarn. Sample DTR 193, Mine 2. Reflected Parallel Polar Light. **i** Gold at the wall of a vug and filling garnet fractures in the *blue-green* garnet skarn. Sample DTR 54b, Mine 2. Reflected parallel polar light

pyroxene in brecciated crystals and as euhedral grains in the quartz matrix.

Clusters and bands, up to a few centimeters in size, of large isotropic to strongly zoned late dark honey-reddish garnet grains (up to 3 mm) of andraditic composition ($Ad_{29–99}$, mean: Ad_{86}, Table 2 and Fig. 9) are observed within and cutting the green pyroxene–epidote skarn, the brown garnet skarn, and the blue-green garnet skarn (Figs. 5a,c,d, and 8e,f), in Mine 2, Southern Sector, and

Table 2 Representative microprobe garnet analyses from the Fortuna mine

Sample	DTR180a_2	DTR132Ab_8	DTR195b_2	DTR122e_6	DTR214b_144	DTR207f_12	DTR218b_9	DTR60a_14	DTR55_24p_13
Location	Mine 2				Cuerpo 3	Southern Sector	Mine 1		Mine 2
Skarn type	Light green pyroxene–garnet skarn	Brown garnet skarn	Blue-green garnet skarn				Dark honey-reddish garnet cluster/vein		
Garnet description	Slightly isotropic grain	Anisotropic grain	Slightly isotropic grain	Anisotropic grain	Anisotropic overgrowth	Anisotropic grain	Isotropic grain		
(wt%)									
SiO_2	38.67	37.50	37.99	36.55	36.65	35.68	34.58	34.65	35.14
Al_2O_3	19.57	15.61	17.83	8.62	10.25	6.52	4.99	0.82	0.00
TiO_2	0.03	0.08	0.99	0.25	1.03	0.01	0.05	0.00	0.01
Fe_2O_3	3.97	10.02	5.45	19.68	16.60	22.79	25.31	30.79	31.43
MnO	1.20	2.40	1.50	1.81	1.77	1.27	0.44	0.90	0.52
MgO	0.07	0.00	0.07	0.00	0.00	0.00	0.00	0.00	0.00
CaO	35.42	33.58	35.47	32.90	33.45	32.77	33.48	32.01	32.83
Total	98.92	99.19	99.30	99.81	99.75	99.04	98.86	99.16	99.94
(Mole fraction)									
Andradite	0.09	0.24	0.13	0.55	0.46	0.67	0.79	0.96	0.99
Grossular	0.88	0.71	0.83	0.41	0.50	0.30	0.20	0.02	0.00
Spessartine	0.03	0.05	0.03	0.04	0.04	0.03	0.01	0.02	0.01

Cr_2O_3 was below detection limit; other end member garnet component=0; all iron is calculated as ferric

Mine 1. Garnet never shows any corrosion at the contact with quartz or later calcite.

Garnet and pyroxene compositions of the Fortuna skarn (Fig. 9) are broadly similar to those of other gold skarns (Meinert 1989). Unlike other mines of the district, a spatial zonation of garnet compositions is apparent in the Fortuna deposit. Garnet reveals iron enrichment from Mine 2 ($Ad_{24–98}$, mean: Ad_{53}) and the Southern Sector, to Cuerpo 3 ($Ad_{68–98}$, mean: Ad_{94}). In addition, the fact that the late dark honey-reddish garnet is more andraditic suggests iron enrichment with time. Pyroxene displays a wide range of compositions ($Hd_{18–40}$, $Di_{47–70}$, $Jo_{7–19}$, Table 3 and Fig. 9).

Table 3 Representative microprobe pyroxene analyses from the Fortuna mine

Sample	DTR207c_2	DTR180h	DTR132a_2	DTR135g_1	DTR214a_4
Location	Southern sector	Mine 2		Cuerpo 3	
Skarn type	Brown garnet skarn	Light green pyroxene–garnet skarn	Blue-green garnet skarn	Light green pyroxene–garnet skarn	
(wt%)					
SiO_2	51.51	52.06	52.12	51.47	51.93
Al_2O_3	0.26	0.19	0.09	0.15	0.15
Fe0	9.44	9.08	8.81	12.20	8.00
MgO	11.27	11.32	11.39	9.06	10.13
MnO	2.34	2.60	3.14	3.30	5.31
CaO	24.07	23.67	24.30	23.59	23.99
Na_2O	0.16	0.17	0.08	0.18	0.06
TiO_2	n.d.	0.02	n.d.	0.02	n.d.
Total	99.04	99.11	99.93	99.97	99.59
(Mole fraction)					
Diopside	0.63	0.63	0.62	0.51	0.58
Hedenbergite	0.29	0.26	0.27	0.38	0.24
Johannsenite	0.08	0.10	0.10	0.11	0.18

Cr_2O_3 was below detection limit
n.d. Not detected

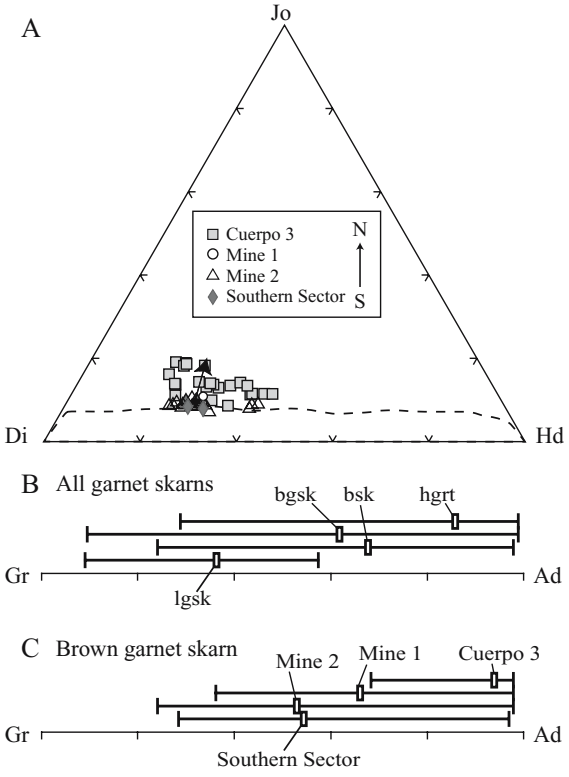

Fig. 9 Pyroxene and garnet composition at Fortuna. **a** Pyroxene is salitic and shows an increase in johannsenite (*Jo*) content from south to north or from proximal to distal position. In general, *Mn* contents are slightly higher than the mean pyroxene composition in gold skarn (*dashed line*) compiled by Meinert (1989). **b** Range and mean garnet composition at Fortuna. *pgsk Green* pyroxene–garnet skarn, *bsk brown* garnet skarn, *bgsk blue-green* garnet skarn, *hgrt dark honey-reddish* garnet. Garnet shows a iron enrichment from massive skarn (*bsk*, *bgsk*, *pgsk*) to late *dark honey-reddish* garnet (*hgrt*). Pyralspite content of all garnet types is less than 5%. **c** Range and mean garnet composition in the *brown* garnet skarn, showing iron enrichment from the proximal zone (Mine 2) to the distal zone (Cuerpo 3)

Increases in MnO (2.5 to 6 wt%) and FeO (7 to 12 wt%, Table 3, Fig. 9) are recognized from the central (Mine 2) to the northern (Cuerpo 3) parts of the studied area.

Skarn relationship with the endoskarn and volcaniclastic rocks

Contacts of the quartz–diorite porphyritic intrusion with the skarn or with volcaniclastic rocks are not exposed in the Fortuna mine due to poor outcrop. Only 25 m separate the northeastern margin of the porphyritic intrusion from the nearest skarn outcrop (Fig. 3). The quartz–diorite suffered in places weak in potassium-silicate alteration with K-feldspar typically mantling plagioclase phenocrysts. Biotite is relatively rare and forms aggregates together with magnetite within and surrounding altered amphibole (Fig. 6a). Irregular, discontinuous vugs are filled with equigranular quartz and K-feldspar (Fig. 6b). Potassium-silicate alteration grades laterally into endoskarn type alteration with development of plagioclase, K-feldspar, epidote, titanite, actinolite, and anhedral fine-grained (<250 μm) pyroxene. Endoskarn alteration assemblages are best recognized in vugs filled with quartz, plagioclase, epidote, magnetite, titanite ± K-feldspar (Fig. 6c). In the groundmass, Na-rich plagioclase partly replaces primary plagioclase. Titanite occurs preferentially within amphibole together with epidote and forms sometimes up to 2.5-mm euhedral crystals. A few millimeters to 1-cm thick quartz ± K-feldspar, pyrite veins (Fig. 5g), which can be assigned to type B veins in the sense of Gustafson and Hunt (1975), crosscut the altered porphyritic intrusion. Potassium-silicate alteration and endoskarn type alterations are overprinted by a weak sericitic alteration. The close spatial relationship of the Fortuna porphyritic intrusion and skarn and the gradational formation of endoskarn suggest that they are genetically related.

Alteration in the volcaniclastic rocks close to the porphyritic intrusion contact and between the massive skarn bodies is similar but more intense than in the intrusion (up to 5-wt% Na_2O and up to 14-wt% CaO, Table 1). Near the porphyritic intrusion contact (sample DTR 156, see Fig. 3) the alteration assemblage consists of Na-rich plagioclase and pyroxene (Fig. 6d), whereas, pyroxene, actinolite ± Na-rich plagioclase and actinolite with rare garnet dominate towards the skarn bodies (samples DTR 194 and DTR 227, see Fig. 3). The increasing abundance of pyroxene, actinolite, epidote ± garnet towards the skarn is expressed first as pockets and bands and then eventually as massive skarn. This mineralogical change is accompanied by a decrease of the Na_2O and increase of the CaO, Cu, and S content towards the skarn (Table 1). The green pyroxene–epidote skarn front typically has a white K-feldspar, Na-rich plagioclase band of several millimeters to centimeters width (Fig. 6e). Analyses of this assemblage display up to 5-wt% K_2O and up to 4.9-wt% Na_2O (Table 1).

Up to 1-mm thick veins filled with fine-grained K-feldspar, pyroxene, quartz, pyrite ± epidote, plagioclase, and chalcopyrite (Fig. 6f,g) crosscut the boundary between skarn and volcaniclastic rocks, and additionally, have garnet on their walls on the skarn side. Late sericitic alteration observed in the quartz–diorite intrusion overprints also locally the altered volcaniclastic rocks and appears to grade laterally into chloritic and/or actinolitic alteration.

Retrograde assemblage, vug fillings, veins, gold occurrence and metal content at Fortuna

As indicated above, retrograde assemblages are mainly located in vugs, elongated vugs and up to centimeter-wide veins. Most veins can be assigned to type I irregular, discontinuous, sulfide-poor veins in the sense of Fontboté et al. (2004). These veins and the vugs are filled with retrograde quartz, epidote, K-feldspar, calcite, and chlorite and minor hematite, pyrite, sericite, apatite, and gold. Type II veins, i.e., veins with similar mineral assemblages but thin (less than 2-mm wide) and throughgoing, are much less common than in other deposits of the district.

Chalcopyrite and sphalerite have been recognized in a type II vein at Mine 1 (Fig. 6i). Rare pyrite-rich throughgoing type III veins with associated sericitic alteration have been observed in Mine 1. In contrast to other mines of the Nambija district (Fontboté et al. 2004) no systematic vein orientation could be observed.

Differences in vug and type I vein infilling minerals were recognized between Mine 1, Mine 2, and the Southern Sector. In Mine 1 vugs, calcite is the main infilling mineral with minor amounts of K-feldspar, chlorite, and quartz (Fig. 5e). In Mine 2, quartz is more abundant than the other infilling minerals (Fig. 5f). In the Southern Sector, vugs are filled mainly by quartz and K-feldspar (Fig. 5c,d). In places, type II veins filled with quartz, K-feldspar, calcite, chlorite, and sphalerite ± chalcopyrite were observed (Fig. 6h,i). When crosscutting vugs, type II vein quartz is in optical continuity with vug quartz (Fig. 6h). A cathodoluminescence study on calcite filling vugs, type I veins, and interstices in the brown garnet skarn (Markowski 2003) reveals similar color (yellow-orange to orange-red) intensities and absence of consistent zonation for all studied calcite grains.

Native gold occurs as interstitial grains, typically up to 100 μm, in places up to 250 μm, between garnet and pyroxene or fills fractured by garnet crystals in skarn affected by retrograde alteration (Fig. 8h and i). It occurs also in vugs, elongated vugs, and type I veins, together with retrograde minerals but is not observed in type II and type III veins. Gold has a relatively low Ag content (5.9- to 14.7-wt%, Table 4) and contains traces of Hg (up to 0.6%).

A striking feature of the Fortuna skarn, similar to most deposits of the Nambija district, is the low content of sulfides (1–3 vol%) and oxides (<1 vol%). Hematite is more abundant in Mine 2, near the N 010° to N 060° E trending Doris and Esteban faults and in the Southern Sector of the mine (where the highest gold grades are observed), whereas,

Table 4 Representative microprobe gold analyses, in weight percent metal, from the Fortuna mine

Sample	DTR 54f	DTR 149a	DTR 175i
Location	Mine 2	Mine 2	Mine 1
Cu	0.05	0.05	0.07
Ag	14.42	7.53	5.91
Au	84.60	92.16	93.86
Hg	0.62	0.53	0[a]
Total	99.70	100.27	99.85

Arsenic, Bi, and Te below detection limit
[a]Detected but not measurable

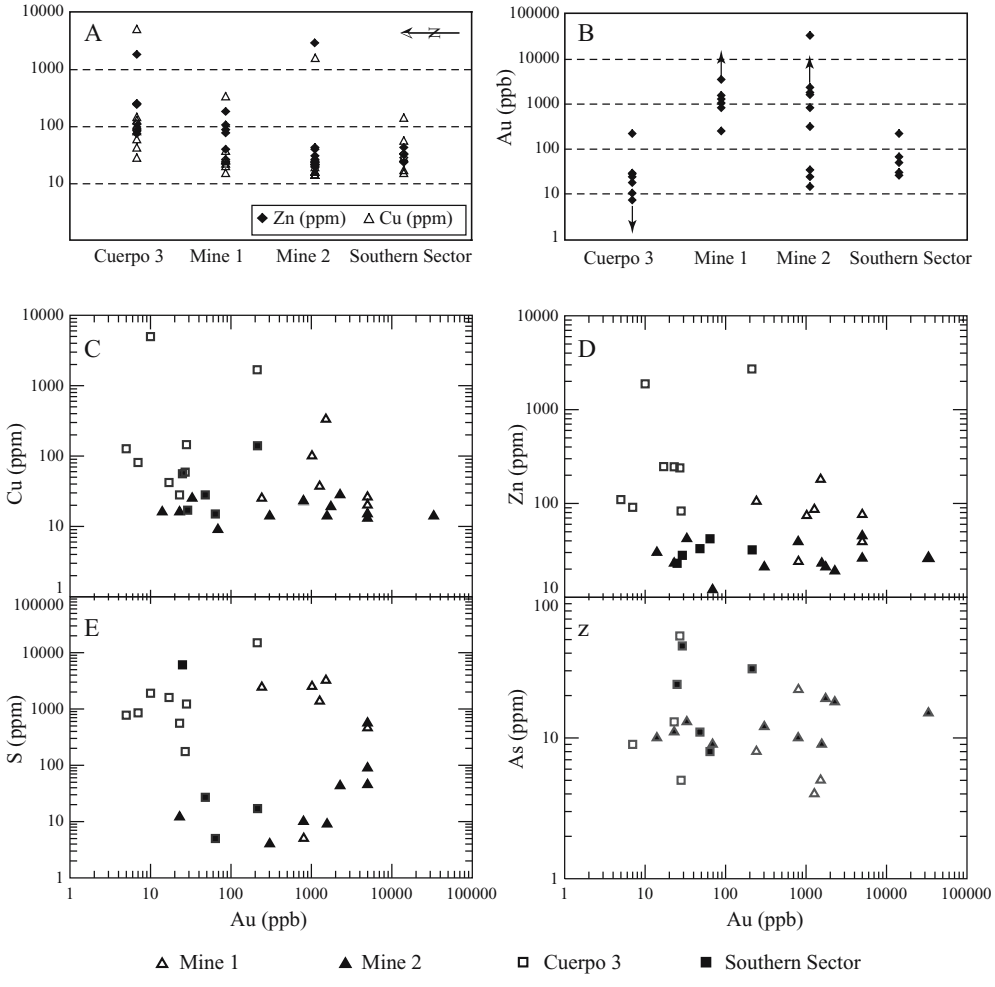

Fig. 10 **a**, **b** Contents of Zn, Cu, and Au, respectively, in selected samples for the Fortuna mine arranged from north to south. Samples of Mine 1 and 2, but one, have, in general, lower Zn–Cu content in average mean than those of Cuerpo 3. *Arrows* indicate values above 5,000-ppb Au **c** Log–log plots of gold vs Cu. **d** Log–log plots of gold vs Zn. **e** Log–log plots of gold versus S. **f** Log–log plots of gold vs As. Content in Zn, Cu, As, and S are similar to the other mines of the Nambija district (Fontboté et al. 2004), but no significant correlation is observed

pyrite is more abundant in Mine 1 and Cuerpo 3 where it can reach 2–3 vol%. Main supergene minerals are pyrolusite, covellite, limonite, and iron hydroxides.

The scarcity of sulfide minerals is reflected in the generally low metal contents of representative mineralized samples (maximum values of selected mineralized samples range around 150-ppm Cu, 300-ppm Zn, 50-ppm As, 2-ppm Te, and 7-ppm Bi, Fig. 10a,c–f and Table 1). Small (~5 μm) bright inclusions within gold grains, suspected to be tellurides, were analyzed with the microprobe. Only in one case was Te above the detection limit (0.36% Te, sample DTR 149, Mine 2, Markowski 2003), so that the presence of tellurides, described in other deposits of the Nambija district (Prodeminca 2000), could not be confirmed. Gold grades show an antithetic distribution with respect to Zn and Cu and are higher (up to 10 ppm) around the Doris and Esteban faults in Mine 2 (Fig. 10b). Gold does not show any correlation neither with S nor with Zn, Cu, and As (Fig. 10c–f). Cu and Zn display the highest values north of Mine 2.

Fluid inclusions and chlorite geothermometry

Fluid inclusions study

Figure 11 presents a compilation of fluid-inclusion data collected on 14 samples (quartz, epidote, garnet, and pyroxene) from the Fortuna mine including 63 data reported by Fontboté et al. (2004) and 22 new data from garnet and epidote minerals. Fluid inclusions in pyroxene ("P" in Fig. 11) were observed in light green pyroxene–garnet skarn in Cuerpo 3. Pyroxene fluid inclusions record high temperature–high salinity fluids (400 to 460°C and 12.8- to 54.5-wt% eq. NaCl). No fluid inclusions in garnet from the volumetrically dominant brown skarn could be observed as it is too turbid and opaque, in part, due to the systematic presence of titanium oxide needles. Primary garnet fluid inclusions from the blue-green garnet skarn ("G1" in Fig. 11) are two phased with salinities ranging from 2.6 to 20.2-wt% eq. NaCl and homogenize to the liquid, critical, or vapor phase between 350 and 475°C without any systematic relationship with salinities. For example, certain high salinity fluid inclusions homogenize to the vapor phase, whereas, certain low salinity fluid inclusions homogenize to the liquid phase. This unsystematic behavior does not support a boiling process. Fluid inclusions in late garnet clusters ("G2" in Fig. 11) are two phased with salinities ranging from 1.0- to 10.1-wt% eq. NaCl and homogenize to the liquid or to the vapor phase between 335 and 405°C.

Primary fluid inclusions in epidote ("E" in Fig. 11) have been found only in epidote-replacing pyroxene in the green pyroxene–epidote skarn and predating late garnet clusters and veins. They display salinities ranging from 5.1 to 19.5-wt% eq. NaCl and homogenization temperatures to the liquid phase between 345 and 425°C.

Quartz grains in blue-green garnet skarn and vugs contain four fluid inclusions types (IA, IB,II, III, Fig. 11). Type IA and type II are, respectively, primary liquid- and vapor-rich fluid inclusions. Both primary inclusion types are found in the same quartz grains indicating that they are coeval. Type IA primary liquid-rich fluid inclusions have moderate salinities (1.6- to 9.7-wt% eq. NaCl) and homogenization temperatures ranging from 180 to 345°C. In places, they contain a transparent rhombohedral solid phase tentatively interpreted as calcite. No microthermometric measurement could be done on type II primary vapor-rich fluid inclusions because of low water content. Type IB are secondary liquid rich fluid inclusions occurring along planes and showing relatively low homogenization temperatures and salinities (125 to 250°C, 0.7- to 2.2-wt% eq. NaCl). Type III are secondary liquid-rich fluid inclusions homogenizing by melting of halite (33- to 35.8-wt% eq. NaCl) with vapor bubble disappearance between 210 and 270°C. Eutectic melting temperatures in garnet, epidote, and quartz fluid inclusions range from −40 to −50°C, indicating the presence of cations like Ca^{2+}, Mg^{2+} or $Fe^{2+/3+}$.

These results are consistent with studies at the scale of the Nambija district (Vallance et al. 2003, Fontboté et al. 2004) and are also consistent with the data of Shepherd (1988) in Litherland et al. (1994) and the observations of Meinert (1998, 2000). However, low temperature (<150°C) and moderate salinity fluid inclusions (5- to 24-wt% eq. NaCl) observed by Shepherd (1988) in Litherland et al.

Type	n =	Mineral	Primary/ Secondary	Tm (°C)	Th (°C)	Mode	Tm KCl (°C)	Tm NaCl (°C)	Salinity wt% NaCl eq
P	8	pyroxene	Primary	-53 to -9	400-460	L	105	280-360	12.8-54.5
G1	23	garnet of the blue-green skarn	Primary (and secondary?)	-17 to -1.5	350-475	L, C or V	-	-	2.6-20.2
G2	16	cluster garnet	Primary	-6.7 to -0.6	335-405	L or V	-	-	1-10.1
E	4	epidote	Primary	-16.1 to -3.1	345-425	L	-	-	5.1-19.5
IA	21	quartz	Primary	-6.4 to -1.2	180-345	L	-	-	9.7-1.6
IB	8	quartz	Secondary	-1.3 to -0.4	125-250	L	-	-	2.2-0.7
II		quartz	Primary	-	-	V	-	-	-
III	5	quartz	Secondary	-29.1 to -26.5	170-215	L	-	210-270	33-35.8

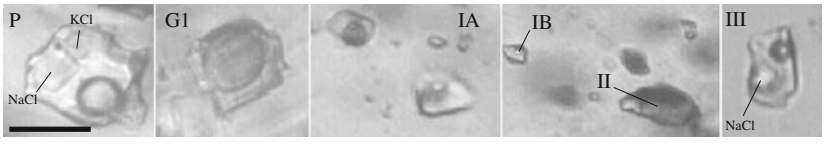

Fig. 11 Compilation of all fluid inclusion data collected in quartz, epidote, garnet, and pyroxene from Fortuna mine and representative photomicrograph of each type. This summary of 85 fluid inclusions includes 65 fluid inclusion data reported by Fontboté et al. (2004) and 22 new data from garnet and epidote minerals. The *black scale bar* represents 10 μm

1994, Vallance et al. (2003), and Fontboté et al. (2004) in quartz and calcite were not observed at Fortuna.

Chlorite geothermometry

Chlorite is an abundant phase of the retrograde mineral assemblage mainly near the Doris and Esteban faults. It occurs as millimeter-sized dark green spots or sometimes as rosettes together with calcite and hematite in green pyroxene–epidote skarn, brown garnet skarn, blue–green garnet skarn, and vugs (Figs. 5c,e,f and 8g).

Chlorite minerals display a broad range of chemical composition, which reflect different physico-chemical conditions of formation, in particular, temperature. Cathelineau and Nieva (1985) and Cathelineau (1988) described an empirical chlorite solid-solution geothermometer based on the positive correlation between tetrahedral alumina and temperature by studying the geothermal systems of Los Azufres (Mexico) and Salton Sea (California). Jowett (1991) proposed a modification to the equation of Cathelineau (1988) based on an isothermal normalization of Cathelineau's data to take into account the variation in Fe/(Fe+Mg). He claimed that this modified geothermometer is applicable in the range 150 to 325°C for chlorite with Fe/(Fe+Mg)<0.6. Kranidiotis and MacLean (1987) also proposed a geothermometer based on a correction of the empirical relationship found by Cathelineau and Nieva (1985). The main constraint of Kranidiotis and MacLean's geothermometer is that chlorite has grown in an Al-saturated environment. De Caritat et al. (1993) have questioned the Fe correction of Kranidiotis and MacLean (1987) because it is based on compositions of chlorites of different generations. This leads to a systematic underestimation of the formation temperature of chlorite (Table 5). The temperatures of chlorite formation at Fortuna calculated with Cathelineau's and Jowett's

Table 5 Representative values from microprobe analyses of chlorites from Fortuna

Label	DTR218a_3	DTR215k_2	DTR122b_3	DTR176a1	DTR149a_2	DTR195c2_8
Location	Mine 1		Mine 2			
Color	Uncolored–pale yellow	Pale yellow	Pale yellowish light green	Light green	Dark green	Dark green
SiO_2	27.21	26.84	24.79	25.05	22.53	23.06
Al_2O_3	17.58	17.80	18.33	18.87	18.89	18.91
FeO	21.75	24.26	35.27	38.41	42.9	42.83
MgO	17.39	15.19	10.2	8.21	4.14	3.48
MnO	3.13	4.13	2.55	1.14	2.71	3.11
Ca_2O	0.11	n.d.	0.01	0.14	0.06	n.d.
Na_2O	n.d.	n.d.	0.01	n.d.	n.d.	n.d.
K_2O	n.d.	0.16	n.d.	0.11	n.d.	0.18
TiO_2	n.d.	0.01	n.d.	n.d.	n.d.	0.04
Total	87.16	88.39	91.15	91.92	91.23	91.61
Structural formula on the basis of 14 oxygen						
Si	2.88	2.85	2.69	2.72	2.57	2.62
Al IV	1.12	1.15	1.31	1.28	1.43	1.38
Al	2.19	2.23	2.35	2.41	2.53	2.52
Al VI	1.07	1.08	1.04	1.13	1.1	1.14
Fe	1.92	2.16	3.2	3.49	4.09	4.06
Mg	2.74	2.41	1.65	1.33	0.7	0.59
Mn	0.28	0.37	0.23	0.10	0.26	0.30
Ca	0.01	0.02	n.d.	0.01	0.01	0.02
Na	n.d.	n.d.	n.d.	n.d.	n.d.	0.01
K	n.d.	n.d.	n.d.	n.d.	n.d.	n.d.
Ti	n.d.	n.d.	n.d.	0.01	n.d.	n.d.
Fe/(Fe+Mg)	0.41	0.47	0.66	0.72	0.85	0.87
T (°C)[a]	300	308	359	352	400	384
T (°C)[b]	303	313	369	364	416	401
T (°C)[c]	168	175	206	208	233	230

All iron is calculated as ferrous. Cr_2O_3 below detection limit
n.d. Not detected
[a]Temperature calculated with Cathelineau's equation (1988)
[b]Temperature calculated with Jowett's equation (1991)
[c]Temperature calculated with Kranidiotis and MacLean's equation (1987)

geothermometers differ by a maximum of 16°C, and are therefore, virtually identical (Table 5). We report in Fig. 12 the temperature values calculated with the Jowett's geothermometer because they allow a direct comparison with data from Hammarstrom (1992) who also used the Jowett's equation.

Hammarstrom (1992) evaluated the formation temperature of chlorite replacing mafic minerals in tuffs from the Piuntza unit and of interstitial chlorite in brown garnet skarn and in garnet–pyroxene–epidote skarn at Nambija. Hammarstrom found temperatures from 165 to 362°C from chlorite with Fe/(Fe+Mg) ranging from 0.24 to 0.32 and interpreted the lowest temperature as resulting from the presence of a smectite component and sometimes to the presence of K-micas. Hammarstrom (1992) proposed that the temperature range between 265 and 290°C is the most representative of chlorite formation.

Chlorites analyzed at Fortuna are from the green pyroxene–epidote skarn (Cuerpo 3 and Mine 1), the brown garnet skarn ± late garnet clusters, the blue-green garnet (±epidote) skarn (Mine 2) and from a vug in the green pyroxene–epidote skarn (Mine 2). Chlorite compositions are variable with Fe/(Fe+Mg) ranging from 0.38 to 0.87. Excluding chlorites with Fe/(Fe+Mg)>0.6 for which Jowett's geothermometer is not applicable, chlorite formation temperatures range from 180 to 350°C with a mode at 330°C (Fig. 12) and only four chlorite analyses indicating temperatures <280°C. Chlorites display similar temperature, between 300 and 340°C, independently from their proximal (Mine 2, 325–335°C) or distal (Mine 1, 305–315°C and Cuerpo 3, 315–325°C) position. The 300–340°C temperature range, representing the temperature range of formation of the great majority of the chlorite minerals at Fortuna, is consistent with the paragenetic association of chlorite with quartz and with the upper temperature range of quartz primary fluid inclusions (up to 345°C).

Discussion and conclusions

The Fortuna skarn appears to be related to the intrusion of the Fortuna quartz-diorite porphyritic intrusion, which crops out in the southern part of the area. We suggest that the skarn has developed largely in volcanic and volcaniclastic rocks of the Triassic Piuntza unit, and perhaps, subordinately, in carbonate rocks, the possible presence of which is only indicated by minor amounts of rocks containing bioclast relicts in Mine 2. An aureole of K–Na metasomatism is observed in the volcaniclastic rocks surrounding the skarn bodies probably because of K and Na mobilization during skarnification.

The Fortuna skarn is of the oxidized type (Zharikov 1970; Burt 1977; Einaudi et al. 1981; Meinert 1989, 1993) with a high garnet:pyroxene ratio, pyroxene being mainly diopsidic and garnet, mainly andraditic. The earliest skarn types are brown garnet skarn and green pyroxene–epidote skarn. The quartz-rich, blue-green garnet skarn, and its light green pyroxene–garnet variety, are interpreted to have formed during the transition between the prograde and retrograde stage.

A zonation of the prograde minerals (pyroxene and garnet) is recognized in terms of mineral composition and mineral abundances but is not as well defined as in other gold skarns hosted by carbonate sequences, which are easier to replace than silica-aluminous rocks (Newberry et al. 1997; L. Meinert 2004, personal communication). The proximal garnet-rich zone is centered on the Doris and Esteban faults in Mine 2, and grades into a distal pyroxene-rich zone to the North (Cuerpo 3, Figs. 3 and 4). Garnet shows iron enrichment from proximal to distal position, in accordance with the systematic zoning in garnet composition of gold-bearing skarns described by Meinert (1997). Iron enrichment with time is also recorded from the massive garnet skarns to the dark honey-reddish garnet clusters. Pyroxene displays also a slight Fe and Mn enrichment towards the Cuerpo 3 in accordance with fluid evolution towards distal zones as described by Meinert (1992) and Nakano (1998). This would again support the proposition of the feeder zone centered in Mine 2 and the

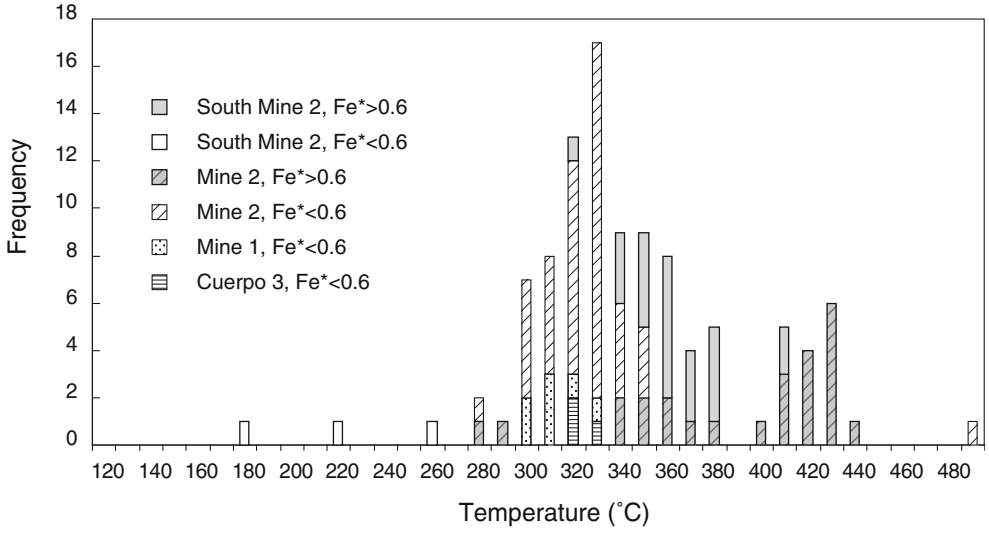

Fig. 12 Histograms of temperatures calculated using the chlorite geothermometer of Jowett (1991) in various sectors of the Fortuna mine. See also Table 5 for typical composition of selected samples

distal part of the system towards the north. Pyroxene is, indeed, richer in manganese than that in other mines of the district (Cambana $Jo_{3–10}$, Campanillas $Jo_{0–12}$, Nambija $Jo_{2–7}$; Guaysimi $Jo_{3–6}$, unpublished data) and in other gold skarns (Meinert 1989; Meinert et al. 2005).

At the Fortuna mine, native gold occurs in the weakly developed retrograde stage of the skarn, together with calcite, quartz, chlorite, hematite, epidote, and K-feldspar within garnet fractures or between mineral joints. This is in agreement with gold occurrence in vugs, as described in Fontboté et al. (2004). Sulfide and oxide contents are very low at Fortuna. Hematite, pyrite, sphalerite, and traces of chalcopyrite have been observed. No molybdenite and tellurides minerals, which have been described in others parts of the district (Litherland et al. 1994; Meinert 1998, 2000; Prodeminca 2000), have been detected. The most Au-rich parts of the skarn are located in the proximal garnet zone near the main 060° Doris and Esteban faults. The highest gold grades coincide also with higher hematite abundance, and generally, with the absence of pyrite suggesting high oxygen fugacity during gold deposition. Farther north, pyrite becomes more abundant and hematite disappears and Zn and Cu content increase in average. These observations suggest that the host rocks in distal zones reduced the oxidized ore-bearing retrograde fluids, or alternatively, this zonation could result from decreasing temperature to the distal zone.

The fact that the retrograde phase is weakly developed and is essentially represented in blue-green garnet skarn, light green pyroxene–garnet skarn, and as open space fillings (containing garnet in apparent paragenetic equilibrium with early quartz), may suggest that the retrograde stage took place at relatively high temperatures in apparent continuum with the prograde stage, as already proposed by Meinert (1998, 2000). This hypothesis is consistent with the homogenization temperatures measured in quartz fluid inclusions (up to 345°C) and those indicated by chlorite geothermometry (up to 340°C).

The highest temperatures (400 to 460°C) and salinities (13- to 54-wt% eq. NaCl) are recorded in pyroxene fluid inclusions and result probably from boiling of a magmatic moderately saline fluid (~8- to 10-wt% eq. NaCl). Slightly lower temperatures found in moderately saline fluid inclusions from garnet and epidote (335 to 475°C) and quartz (<345°C) represent the beginning of the retrograde stage and are consistent with the chlorite geothermometry results (300 to 340°C).

Fluid inclusions and chlorite geothermometry suggest that gold deposition occurred around 300°C. Significant gold transport as hydrosulfide complexes is unlikely, taking into account the oxidizing nature of the fluid as indicated by the association of the main mineralized areas with hematite and by the scarcity of sulfides. Very low metal contents also point to a fluid poor in reduced sulfur. Consequently, gold was more likely transported in the form of chloride complexes and deposition occurred mainly in the proximal zone, after cooling below 300°C when transport of chloride complexes as gold carriers is not efficient (Gammons and Williams-Jones 1997). The phenomena could be enhanced by neutralization of the weakly acid fluid (K-feldspar stable) during hydrolysis of the prograde calc-silicate assemblage as suggested by the formation of sericite and calcite at this stage.

Skarn types, mineral composition and abundance, paragenetic sequence, and fluid evolution is similar to that observed in the other mines of the Nambija district by Fontboté et al. (2004). However, Fortuna is the only mine of the district where a well-defined mineralogical zonation could be recognized at the mine scale and the feeder zone identified. Unlike Campanillas, Nambija, and Guaysimi (Fontboté et al. 2004) at the Fortuna veining is poorly developed with rare type I veins of several millimeters thickness and a relative dissemination of gold mineralization in vugs located around the N 060° E Doris and Esteban faults. Bonanza zones with native gold-building grains up to several millimeters in sizes, which are commonly observed at Campanillas, Nambija, and Guaysimi, are absent at Fortuna. Post-skarn, sulfide-rich type III veins and associated sericitic alteration are less developed than in other deposits of the district.

Like in other skarn deposits worldwide, at Fortuna, gold deposition occurred during the retrograde stage. The main difference with other high-grade gold skarn is its oxidation state at the time of gold deposition (hematite stable). The largest high-grade gold skarns like Fortitude in Nevada (Myers 1994; Doebrich and Theodore 1996; Doebrich et al. 1996) or Hedley in British Columbia (Ray et al. 1996) are of the reduced type (Meinert 1998, 2000). They show prograde mineral assemblages lacking ferric iron with high hedenbergitic pyroxene:granditic garnet ratio. Gold deposition occurs in the distal pyroxene-rich zone during the retrograde stage, together with a large amount of sulfides. Moreover, As, Bi, and Te minerals are common. Bismuth minerals are typically found in reduced gold skarns in association with sulfides, arsenic minerals, and gold ores while they are less abundant (as As minerals) in oxidized gold skarns (Meinert 2000). Skirrow and Walshe (2002) suggest that Bi, As, and Sb show a similar behavior in hydrothermal fluids and that deposition is favored by reduction. The Fortuna skarn shows more similarities with the McCoy skarn, likewise defined as pertaining to the oxidized type (Brooks 1994; Brooks et al. 1991; Meinert 1998, 2000). The McCoy gold skarn shows a mineralogical zonation with an aluminous garnet-rich proximal zone and a diopsidic pyroxene-rich distal zone. Gold mineralization is spatially associated with the proximal zone and occurred during retrograde alteration consisting mainly of epidote–quartz–pyrite–K-feldspar together with pyrrhotite as sulfide mineral. Although relatively low, total sulfides and Bi–Te minerals content at McCoy is higher than at Fortuna and hematite is absent. Moreover, low vein density, absence of stockworks or breccias and weak retrograde alteration at Fortuna suggests that quartz–diorite emplacement and skarn formation occurred at a deeper level than at McCoy. Similar to Fortuna, Wabu (Irian Jaya) is an oxidized gold skarn, dominated by garnet, where gold mineralization occurs in the proximal zone, together with retrograde K-feldspar (Allen and Aslund 1998). However,

the protolith in Wabu is calcareous, and gold occurs together with pyrrhotite, arsenopyrite, and bismuth. At McCoy and Wabu, the presence of pyrrhotite indicates that the conditions of gold deposition were reducing and the temperature of deposition occurred at about 300 to 400°C. Hence, the particularity of Fortuna is that the oxidizing conditions persisted at a lower temperature than at McCoy and Wabu (<300–350°C), which prevented gold-sulfide association and did not allow the deposition of significant amounts of Bi–Te minerals.

Acknowledgements This work was supported by the Swiss National Science Foundation project n° 2000-062 000.00, the Académie Suisse des Sciences Naturelles, and the Society of Economic Geologists grants. We thank Fortuna Gold Mining Corp, Quito, Ecuador, for granting access to the Fortuna mine. Tom Shepherd and Fernando Tornos are also acknowledged for discussion and suggestions. This paper benefited from the fruitful comments of J. Hammarstrom, S. Redwood, L. Meinert, and D. Lentz.

Appendix

Representative whole rock compositions (XRF analyses) of Triassic volcaniclastic rocks (TVR), later porphyry intrusions (PI), and dikes Oxides, weight percent; trace elements, parts per million

Sample	DTR 156	DTR 194	DTR 221	DTR 233	DTR 184	DTR 391	DTR 399b	DTR 69	DTR 378	DTR 417	DTR 361-2	DTR 373	DTR 405
Location	Fortuna Southern Sector	Fortuna Mine 2	Fortuna Mine 1	Fortuna Southern Sector	Fortuna Southern Sector	Access road to Cambana	Access road to Cambana	Campanillas–Katy	Nambija–Mapasingue	Road to Nambija	Guaysimi–Central	Guaysimi–Central	Guaysimi
Rock type	TVR	TVR	Dike	Dike	PI	PI	TVR	PI	TVR	PI	TVR	TVR	TVR
SiO_2 (wt%)	62.37	62.69	44.70	44.91	63.45	62.48	54.66	60.51	71.12	61.41	58.10	58.25	55.40
TiO_2	0.48	0.35	0.86	0.97	0.41	0.53	0.74	0.52	0.36	0.52	1.05	0.83	0.74
Al_2O_3	16.22	11.60	15.26	16.25	17.29	17.67	17.38	17.33	13.13	17.18	18.19	16.91	18.55
Fe_2O_3[a]	4.98	5.31	9.72	11.20	4.25	4.64	3.51	3.38	2.55	4.81	1.39	1.40	4.76
MnO	0.05	0.39	0.76	0.44	0.14	0.13	0.24	0.12	0.02	0.06	0.32	0.14	0.13
MgO	0.87	0.10	8.56	9.22	1.14	1.99	5.77	1.71	0.15	1.61	2.34	3.64	3.15
CaO	1.26	13.90	10.22	8.14	4.53	1.57	5.90	4.97	0.08	5.57	7.52	8.24	0.57
Na_2O	4.86	0.07	2.26	1.62	3.71	4.08	2.23	5.33	2.77	4.05	6.37	5.57	4.86
K_2O	5.04	4.67	1.84	2.4	2.93	3.04	4.62	3.57	6.86	2.96	1.74	2.42	2.70
P_2O_5	0.09	0.20	0.16	0.19	0.17	0.16	0.17	0.19	0.06	0.23	0.20	0.10	0.12
LOI	2.80	0.02	4.81	0.07	1.32	2.98	3.52	1.78	1.03	1.16	1.14	1.83	4.26
Nb (ppm)	6	4	2	1	6	6	3	4	11	4	2	2	4
Zr	87	46	32	30	100	119	107	85	321	88	105	67	127
Y	23	20	18	22	23	20	29	23	28	28	14	38	28
Sr	140	40	253	379	571	302	89	347	15	620	167	267	147
U	3	3	3	<2	<2	5	3	<2	4	3	4	6	3
Rb	89	68	64	97	63	82	133	80	118	56	86	85	103
Th	8	2	4	<2	4	9	6	5	13	7	6	6	5
Pb	11	12	14	8	5	5	9	8	10	8	<2	4	5
Ga	17	10	18	16	18	18	17	19	14	17	10	16	23
Zn	23	12	237	98	35	51	142	32	19	18	29	30	86
Cu	1,440	9	130	102	17	9	11	168	4	6	7	5	38
Ni	3	<2	43	44	2	<2	6	<2	2	<2	7	31	5
Co	30	71	37	49	46	17	13	41	80	33	17	13	14
Cr	12	26	158	119	8	8	29	10	15	8	17	37	19
V	99	81	425	414	66	101	175	124	25	93	71	346	156
Ce	36	8	19	15	25	42	26	32	20	33	31	23	42
Nd	17	0	10	6	13	23	18	16	13	20	17	18	21
Ba	1,197	1,638	963	3,725	971	1,215	788	819	563	1,220	172	824	513
La	17	<4	8	<4	16	19	11	20	10	24	17	16	20
S	9,273	<3	1,727	7	<3	41	54	5,831	1,935	<3	77	167	20
Hf	16	8	2	2	6	6	5	5	7	6	6	2	5
Sc	5	2	41	45	6	7	10	6	3	8	10	8	20
As	5	9	8	8	7	8	5	<3	6	4	8	19	30

TVR Triassic volcaniclastic rock, *PI* porphyric intrusion, *LOI* loss on ignition
[a]Total Fe as Fe_2O_3

References

Allen J, Aslund T (1998) The Wabu gold skarn, Irian Jaya, Indonesia: the Gangue, newsletter of the mineral deposit division. Geol Assoc Can 59:9–11

Bakker RJ, Brown PE (2003) Computer modeling in fluid inclusion research. In: Ian Samson, Alan Anderson, Dan Marshall (eds) Fluid inclusion analysis and interpretation. Min Assoc Can Short Course Series 32:175–212

Bodnar RJ, Vityk MO (1994) Interpretation of microthermometric data for H_2O–NaCl fluid inclusions. In: De Vivo B, Frezzotti ML (eds) Fluid inclusions in minerals, methods and applications. Virginia Tech, Blacksburg, VA, pp 117–130

Brooks JW (1994) Petrology and geochemistry of the McCoy gold skarn, Lander County, Nevada. Ph.D. thesis, Washington State University, Pullman, Washington, p 607

Brooks JW, Meinert LD, Kuyper BA, Lane ML (1991) Petrology and geochemistry of the McCoy gold skarn, Lander County, NV. In: Raines GL, Lisle RE, Schafer RW, Wilkinson WH (eds) Geology and ore deposits of the great basin. Geological Society Nevada, Reno, pp 419–442

Burt DM (1977) Mineralogy and petrology of skarn deposits. Soc It Min Pet Rend 33:859–873

Cathelineau M (1988) Cation site occupancy in chlorites and illites as a function of temperature. Clay Miner 23:471–485

Cathelineau M, Nieva D (1985) A chlorite solid solution geothermometer. The Los Azufres geothermal system (Mexico). Cont Miner Pet 91:235–244

de Caritat P, Hutcheon I, Walshe JL (1993) Chlorite geothermometry: a review. Clays clay miner 23:219–239

Doebrich JL, Theodore TG (1996) Geologic history of the Battle Mountain mining district, Nevada, and regional controls on the distribution of mineral systems. In: Coyner AR, Fahey PL (eds) Geology and ore deposits of the American Cordillera. Geological Society Nevada, Reno, pp 453–483

Doebrich JL, Wotruba PR, Theodore TG, McGibbon DH, Felder RP (1996) Field trip guidebook for Trip H—geology and ore deposits of the Battle Mountain mining district. In: Green SM, Struhsacker E (eds) Field trip guidebook compendium. Geological Society Nevada, Reno, pp 327–388

Einaudi MT, Meinert LD, Newberry RJ (1981) Skarn deposits. Econ Geol 75:317–391

Feininger T (1987) Allochthonous terranes in the Andes of Ecuador and northwestern Peru. Can J Earth Sci 24:266–278

Fontboté L, Vallance J, Markowski A, Chiaradia M (2004) Oxidized gold skarns in the Nambija District, Ecuador. In: Perrello J, Sillitoe R, Vidal C (eds) Andean metallogenesis. SEG Special Publication 11:341–357

Gammons CH, Williams-Jones AE (1997) Chemical mobility of gold in the porphyry-epithermal environment. Econ Geol 92:45–59

Gendall IR, Quevedo LA, Sillitoe RH, Spencer RM, Puente CO, Leon JP, Povedo RR (2000) Discovery of a Jurassic porphyry copper belt, Pangui area, southern Ecuador. SEG Newsletter 43 (1):8–15

Gustafson LB, Hunt JP (1975) The porphyry copper deposit at El Salvador, Chile. Econ Geol 70:856–912

Hammarstrom JM (1992) Mineralogy and chemistry of gold-associated skarn from Nambija, Zamora Province, Ecuador: a reconnaissance study. Adv US Int Min Res USGS 107–118

Hughes RA, Pilatasig LF (2002) Cretaceous and Tertiary terrane accretion in the Cordillera Occidental of the Andes of Ecuador. Tectonophysics 345:29–48

Jaillard E, Benitez S, Mascle GH (1997) Les déformations paléogènes de la zone d'avant-arc sud équatorienne en relation avec l'évolution géodynamique. Bull Soc Geol Fr 168:403–412

Jowett EC (1991) Fitting iron and magnesium into the hydrothermal chlorite geothermometer. GAC/MAC/SEG Joint Annual Meeting (Toronto). Program with Abstracts 16, p 62

Kranidiotis P, MacLean WH (1987) Systematics of chlorite alteration and the Phelps Dodge massive sulfide deposit. Matagami, Quebec. Econ Geol 82:1898–1992

Litherland M, Fortey NJ, Beddoe-Stephens B (1992) Newly discovered Jurassic skarn fields in the Ecuadorian Andes. J South Am Earth Sci 6:67–75

Litherland M, Aspden JA, Jemielita RA (1994) The metamorphic belts of Ecuador. BGS, Overseas Memoir 11, Keyworth UK, p 147

Markowski A (2003) The gold skarn of Fortuna, (Nambija District, Cordillera del Cóndor, Ecuador). Ms thesis, University of Geneva, 184 p. Also accessible on line under http://www.unige.ch/sciences/terre/mineral/

McKelvey GE, Hammarstrom JM (1991) A reconnaissance study of gold mineralization associated with garnet skarn at Nambija, Zamora Province, Ecuador. In: Good EJ, Slack JF, Kotra RK (eds) USGS research on mineral resources—1991, program and abstracts. US Geol Surv Circ, vol 1062, p 55

Meinert LD (1989) Gold skarn deposits—geology and exploration criteria. In: Groves DI, Keays R, Ramsay R (eds) Proceedings of Gold '88, Economic Geology Monographs, vol 6. pp 537–552

Meinert LD (1992) Skarns and skarn deposits. Geosci Can 19: 145–162

Meinert LD (1993) Igneous petrogenesis and skarn deposits. In: Kirkham RV, Sinclair WD, Thorpe RI, Duke JM (eds) Geol Assoc Can Special paper 40:569–583

Meinert LD (1997) Application of skarn deposit zonation models to mineral exploration. Explor Min Geol 6:185–208

Meinert LD (1998) A review of skarns that contain gold. In: Lentz DR (ed) Mineralized porphyry/skarn systems. Min Assoc Can Short Course Series, 26:359–414

Meinert LD (2000) Gold in skarns related to epizonal intrusions. In Hagemann SG, Brown PE (eds) Gold in 2000. Rev Econ Geol 13:347–375

Meinert, LD, Dipple, GM, and Nicolescu, S (2005) World Skarn Deposits: in Hedenquist, JW, Thompson, JFH, Goldfarb, RJ, and Richards, JP (eds) Economic geology 100th anniversary volume, society of economic geologists, Littleton, Colorado, USA, includes supplementary appendices on CD-ROM (filename: Meinert), pp 299–336

Mining Magazine (1990) Campanilla gold mine. Min Mag 163: 322–323

Myers GL (1994) Geology of the Copper Canyon–Fortitude skarn system, Battle Mountain, Nevada. Ph.D. thesis, Washington State University, Pullman, p 356

Nakano T (1998) Pyroxene geochemistry as an indicator for skarn metallogenesis in Japan. In: Lentz DR (ed) Mineralized porphyry/skarn systems. Mineral Assoc Can Short Course Series 26:147–167

Newberry RJ, Allegro GL, Cutler SE, Hagen-Leveille JH, Adams DD, Nicholson LC, Weglarz TB, Bakke AA, Clautice KH, Coulter GA, Ford MJ, Myers GL, Szumigala DJ (1997) Skarn deposits of Alaska. In: Goldfarb RJ (ed) Ore Deposits of Alaska. Econ Geol Monogr 9:355–395

Paladines A, Rosero G (1996) Zonificación mineralogénica del Ecuador: Ed. Laser, Quito, p 146

Pearce JA, Harris NBW, Tindle AG (1984) Trace element discrimination for the tectonic interpretation of granitic rocks. J Petrol 25:956–983

Prodeminca (2000) Depósitos porfídicos y epi-mesotermales relacionados con intrusiones de la Cordillera del Cóndor: Evaluacion de distritos mineros del Ecuador: UCP Prodeminca Proyecto MEM BIRF 36-55 EC 5

Ray GE, Dawson GL, Webster ICL (1996) The stratigraphy of the Nicola Group in the Hedley district, British Columbia and the chemistry of its intrusions and Au skarns. Can J Earth Sci 33:1105–1126

Shepherd TJ (1981) Temperature programmable heating-freezing stage for microthermometric analysis of fluid inclusions. Econ Geol 76:1244–1247

Skirrow RG, Walshe JL (2002) Reduced and oxidised Au–Cu-Bi iron–oxide deposits of the Tennant Creek Inlier, Australia; an integrated geologic and chemical model. Econ Geol 76: 1167–1202

Sterner SM, Bodnar RJ (1984) Synthetic fluid inclusions in natural quartz. I. Compositional types synthesized and applications to experimental geochemistry. Geochim Cosmochim Acta 48: 2659–2668

Sterner SM, Hall DL, Bodnar RJ (1988) Synthetic fluid inclusions. V. Solubility relations in the system NaCl–KCl–H_2O under vapor-saturated conditions. Geochim Cosmochim Acta 52: 989–1006

Vallance J, Markowski A, Fontboté L, Chiaradia M (2003) Mineralogical and fluid inclusion constraints on the genesis of gold-skarn deposits in the Nambija district (Ecuador). In: Eliopoulos D et al (eds) Proc. of Seventh Biennal SGA Meeting, Mineral exploration and sustainable development, Millipress, Athens Greece, pp 399–402

Winchester JA, Floyd PA (1976) Geochemical magma type discrimination: application to altered and metamorphosed basic igneous rocks. Earth Planet Sci Lett 28:459–469

Zharikov VA (1970) Skarns. Int Geol Rev 12:541–559, 619–647, 760–775